

New Spectral Compensation Method for Intercalibration Using High Spectral Resolution Sounder

TAHARA Yoshihiko* and KATO Koji*

Abstract

For intercalibration between a broadband channel like an imager channel on a geostationary satellite and a high spectral resolution sounder (hyper sounder), a super channel consisting of the channels of the hyper sounder (hyper channels) is used. If there are failed channels, spectral gap and shortage contained in the hyper sounder, accuracy for the super channel to simulate the broadband channel degrades. The spectral compensation is important for the intercalibration using that hyper sounder. First, this study introduces virtual channels named *gap channels*. Using the gap channels in addition to the hyper channels including failed channels, the super channel can be generated to have a spectral response nearly the same as that of the geostationary channel. Second, this study introduces a spectral compensation method based on the spectral information with respect to eight atmospheric model profiles. The radiances of the missing channels are calculated by regression analysis using the beforehand radiative transfer simulated radiances with respect to the atmospheric model profiles including clear and cloudy weather conditions over the Tropics and mid latitude. The regression coefficients are computed by applying validly observed radiances of the hyper channels to the response variable. Finally, the radiance of super channel is computed by using the hyper sounder observed radiances in addition to the calculated ones for the missing channels. The advantage of this method is that it does not use radiative transfer computation and numerical weather prediction fields in operation. The radiance of the super channel is computed without introducing biases originating from the numerical weather prediction fields and the radiative transfer computation. Furthermore, this method is applicable to cloudy weather conditions. To validate the spectral compensation technique, the missing channels of AIRS are simulated by IASI channels, and the spectral compensation is also examined for these IASI channels. Improvement to reduce systematic biases arising from the missing channels is recognized by using this spectral compensation technique in the validations of all infrared channels of MTSAT-1R, METEOSAT-8 and GOES-12. The two-month comparison of the MTSAT-1R infrared channels against the AIRS super channels also shows good agreement with the comparison against the IASI super channels by using this compensation technique.

* System Engineering Division, Data Processing Department, Meteorological Satellite Center
(Received July 31, 2008, Accepted January 22, 2009)

1 Introduction

It is important to study the calibration accuracy of space-based sensors after launch. Intercalibration, which is conducted by comparing observed data between two or more sensors, is one solution for the study. The information obtained from the intercalibration is useful for monitoring and reviewing the hardware and software of the sensors and assisting satellite data users.

The Global Space-Based Inter-Calibration System (GSICS) is an international project to examine the intercalibration with respect to operational satellites by unified algorithms and produce consistent calibration information. As a reference for the intercalibration of infrared channels of imagers aboard geostationary satellites, the GSICS employs a high spectral resolution sounder (hereinafter called a *hyper*

sounder), which observes radiance exiting from the top of the atmosphere over a wide infrared spectral region with a large number of narrow bandwidth channels (hereinafter called *hyper channels*).

Currently, there are two hyper sounders operated and used by the GSICS infrared intercalibration. The Atmospheric Infrared Sounder (AIRS) is a hyper sounder launched by the National Aeronautics and Space Administration (NASA) aboard the satellite AQUA in 2002. The Infrared Atmospheric Sounding Interferometer (IASI) is another hyper sounder launched by the European Organization for the Exploitation of Meteorological Satellites (EUMETSAT) aboard the satellite METOP-A in 2006.

Figure 1 shows the flow of the infrared intercalibration system of the MTSAT-1R imager, which carries broadband infrared

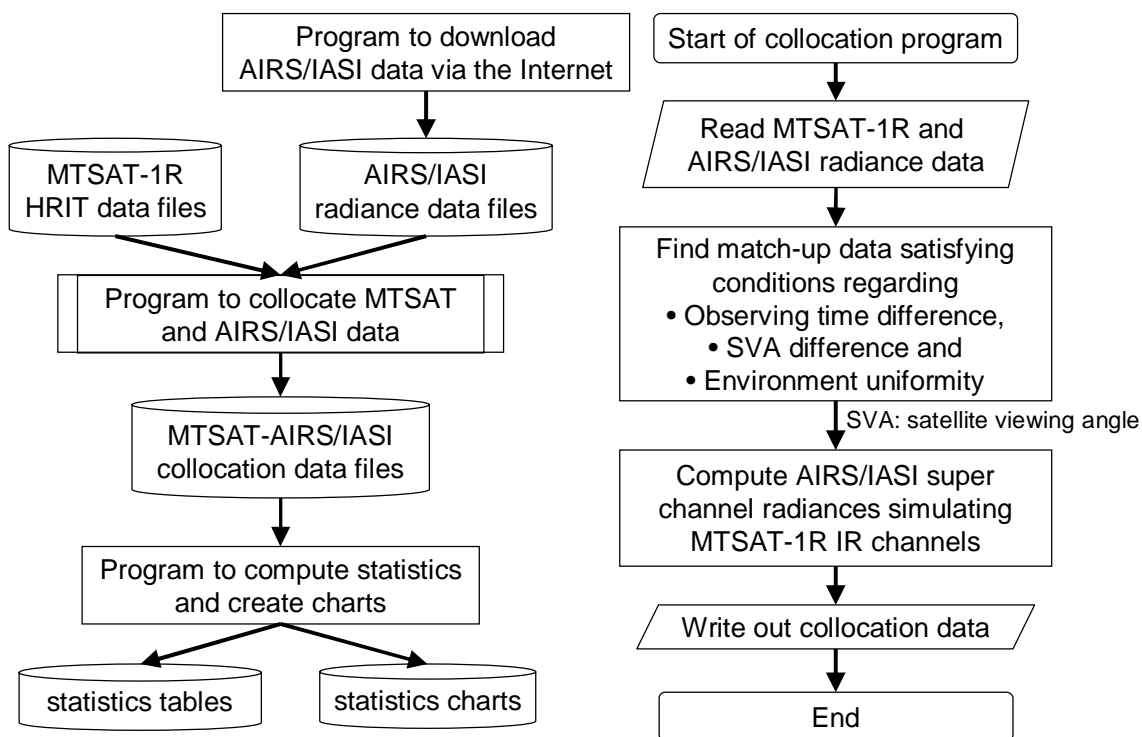


Figure 1: Flow chart of the infrared intercalibration system of the MTSAT-1R imager with AIRS and IASI.

channels, with the hyper sounders, AIRS and IASI. The main flow is shown on the left diagram. There are three programs; downloading hyper sounder radiance data, collocating data between the MTSAT-1R imager and hyper sounder, and generating statistics and charts. The flow of the collocation program is displayed on the right diagram. There are two computation steps. The first step is to find match-up data between MTSAT-1R and the hyper sounders by inspecting observed time difference, satellite viewing angle difference and horizontal environment uniformity. The second step is to simulate the radiance of the broadband channel from hyper sounder radiance data. For the radiance simulation, a super channel, which is generated by accumulating hyper channels, is introduced.

Tahara (2007) generates the super channels introducing the *constraint method* to obtain a spectral response whose difference from the broadband channel is minimized. The super channel simulates the broadband channel accurately only if the hyper sounder fully covers the spectral band of the broadband channel. However, the AIRS spectral band includes some gaps, and the spectral ranges of AIRS and IASI are not wide enough to cover the bands of some geostationary channels. In addition, some AIRS channels have failed, and their observations are not usable. These spectral gaps and shortages prevent accurate simulation by the hyper sounder. This report proposes a new method to compensate for the spectral gaps and shortages involved in the super channel.

2 Methodology

This section introduces the methodology of the spectral compensation. Section 2.1 reviews the spectral response of the super channel generated from the hyper channels and the effect of spectral gaps and failed channels involved in the hyper sounder. Section 2.2 introduces virtual channels named *gap channels* to fill the spectral gaps. Section 2.3 introduces a method to compensate for the radiances of the missing (failed and gap) channels by a regression approach. Section 2.4 shows a procedure to compute super channel radiances applying the spectral compensation method to use missing channel calculated radiances in addition to hyper sounder observed ones.

In this section, examples and charts with respect to MTSAT-1R channel IR3 ($6.8 \mu\text{m}$) and AIRS are mainly presented for the explanation of the methodology. Because AIRS has two spectral gaps over the IR3 spectral region, where spectral compensation is very difficult due to a lot of strong water vapor absorption lines. With respect to other MTSAT-1R imager channels as well as METEOSAT-8 and GOES-12 channels, additional charts for those channels are presented in the Appendix.

2.1 Super channel

The *constraint method* (Tahara, 2007) introduces a super channel accumulating hyper channels to simulate a broadband channel. The intercalibration using hyper sounder is examined to compare radiance of the super channel with that of the broadband channel.

The constraint method computes the

radiance of the super channel I_s by linearly accumulating radiances of hyper channels I_i , where i denotes the hyper channel index number,

$$I_s = \frac{\sum_i w_i I_i}{\sum_i w_i}. \quad (1)$$

w_i represent super channel weights, which are computed by minimizing difference between the spectral response function (SRF) of the super channel $S_s(\nu)$ and that of the broadband channel $S_b(\nu)$ to satisfy the approximation,

$$S_b(\nu) \approx S_s(\nu) = \sum_i w_i S_i(\nu). \quad (2)$$

$S_i(\nu)$ is the SRF of the hyper channel i . $S_b(\nu)$ and $S_i(\nu)$ used in (2) are normalized for their areas to be one,

$$\int S_i(\nu) d\nu = \int S_b(\nu) d\nu = 1.$$

The super channel of the constraint method simulates the broadband channel with high accuracy in case the hyper sounder fully covers the spectral band of the broadband channel. However, the approximation in (2) degrades if there are spectral gaps and shortages.

Figure 2 shows the SRF of an AIRS super channel (green lines) simulating MTSAT-1R

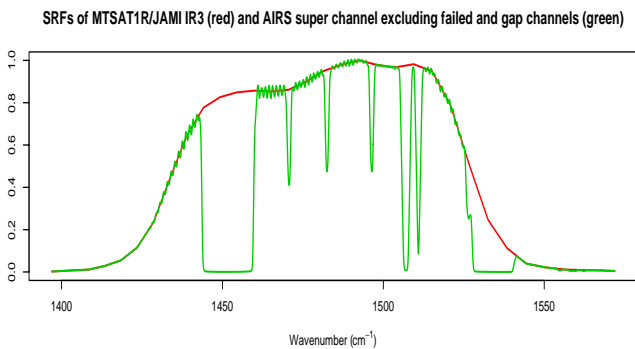


Figure 2: SRFs of the MTSAT-1R channel IR3 (6.8 μm) (red lines) and its super channel generated by the constraint method from AIRS channels excluding failed channels (green lines).

channel IR3 (6.8 μm) (red lines). Since the AIRS spectral coverage contains wide gaps around 1450 cm^{-1} and 1530 cm^{-1} , the super channel SRF drops there. Other narrow drops are observed, since AIRS failed channels are excluded from the super channel.

The same charts as Figure 2 but for other geostationary imager channels are presented in Chart (e) of the figures in the Appendix. The SRF discrepancy of AIRS/IASI super channels from the simulating image channels are also recognized as the AIRS super channel of IR3. This discrepancy is anticipated to cause systematic bias in super channel radiance. To reduce the bias, such spectral gaps and shortages involved in the hyper sounder should be compensated for.

2.2 Gap channels

The green shaded areas in Figure 3 (a) represent the spectral observing coverage of the AIRS 2378 channels. AIRS covers the spectra from 650 to 2665 cm^{-1} including some gaps between the AIRS detector modules. Figure 3 (c) shows the SRFs of the MTSAT-1R, METEOSAT-8 and GOES-12 infrared channels. Some of the AIRS spectral gaps lie within the bands of these geostationary infrared channels. In addition, the AIRS spectral range does not fully cover the bands of MTSAT-1R channel IR4 (3.8 μm) and METEOSAT-8 3.9 μm channel.

The green shaded area in Figure 3 (b) represents the spectral observing coverage of the IASI 8461 channels. IASI covers the spectra from 645 to 2730 cm^{-1} . Unlike AIRS, there is no spectral gap. However, IASI, like AIRS, does not fully cover the spectral band of MTSAT-1R channel IR4 and METEOSAT-8 3.9 μm .

As mentioned in Section 2.1, the spectral gaps and shortages are expected to degrade the super channel and therefore need to be compensated for. To fill the spectral gaps and shortages, virtual channels named *gap channels* are first introduced.

The gap channels to fill the AIRS spectral gaps and shortages (*AIRS gap channels*) are defined by 0.5 cm^{-1} intervals, and are characterized by a unique SRF, whose shape is a Gaussian curve with a sigma of 0.5 cm^{-1} . The orange shaded areas in Figure 3 (a) show spectra filled by the AIRS gap channels. Figure 4 shows examples of the SRFs of the AIRS channels and gap channels.

The gap channels to extend the IASI spectral

region (*IASI gap channels*) are defined by the same intervals (0.25 cm^{-1}) and SRFs as the IASI level 1c channels. The orange shaded areas in Figure 3 (a) show spectra filled by the AIRS gap channels. Figure 5 shows an example of the SRFs of the IASI channels and gap channels.

Using the gap channels with hyper channels including failed channels, the super channel can be generated to have a SRF very close to the broadband SRF. Figure 6 (a) shows the same chart as Figure 2, but the super channel includes AIRS failed and gap channels. The super channel SRF (green lines) is entirely corresponding to the IR3 SRF (red lines) with small variation. Simulated brightness

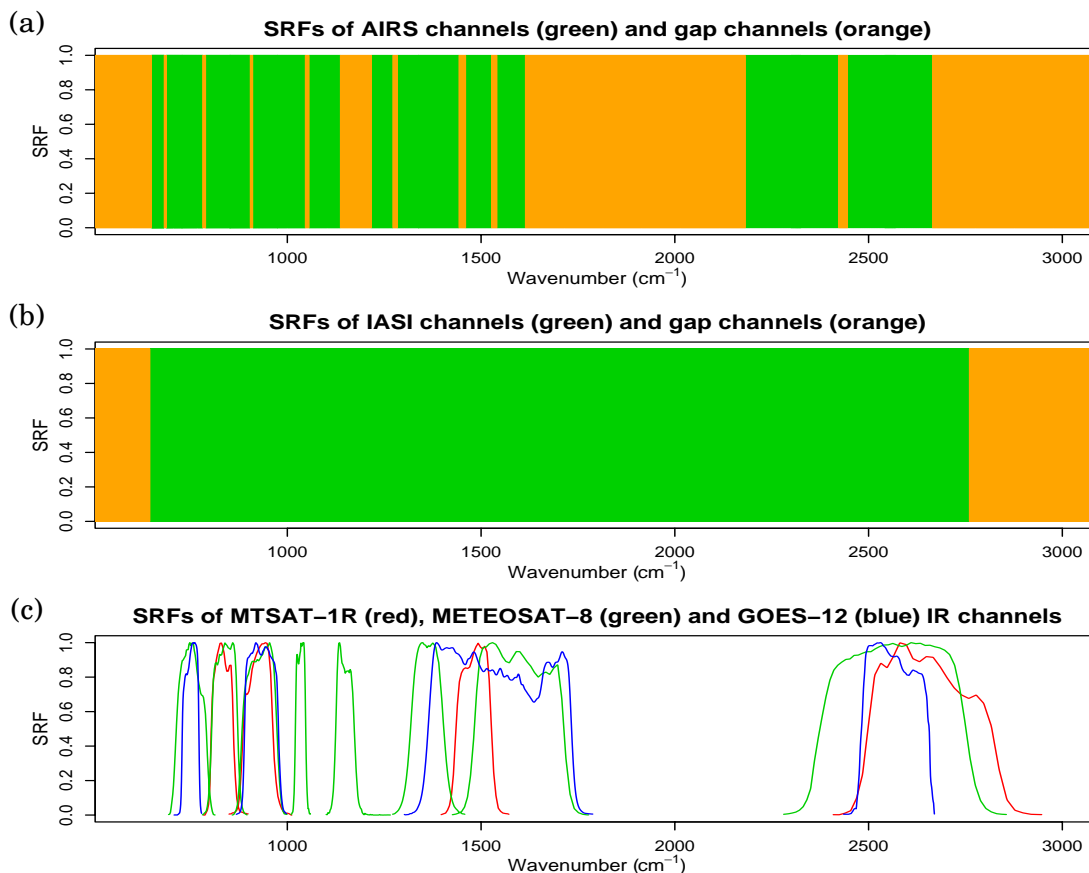


Figure 3: (a) shows spectral of AIRS channels (green area) and AIRS gap channels (orange area). (b) shows that of IASI channels (green area) and IASI gap channels (orange area). (c) shows SRFs of MTSAT-1R (red lines), METEOSAT-8 (green lines) and GOES-12 (blue lines) infrared channels.

temperature difference between IR3 and the super channel is less than 0.01 K with respect to the United States standard profile.

Figure 6 (b) shows the weights of the super channels. The green, purple and orange lines represent the weights of the AIRS valid, failed and gap channels, respectively. There are 267 AIRS valid channels, 26 failed channels and 60 gap channels. The sequence of the weights curves is very similar to the shape of the IR3 SRF. Some variation is observed, since the super channel is generated by minimizing the

difference of the approximation in (2), and this minimization does not assure the smoothness of the sequence.

The SRFs and weights of the super channels to simulate other geostationary imager channels are shown in Charts (a) and (b) of the figures in the Appendix. The SRFs are well correlated to those of simulating imager channels, whereas the weights show some variations, as similarly recognized for the AIRS super channel of IR3 in Figure 6 (a) and (b).

2.3 Compensation for missing channels

The good agreement of SRFs between the super channel and the broadband channel shown in Figure 6 (a) indicates that the observed information of the broadband channel can be simulated by using the super channel

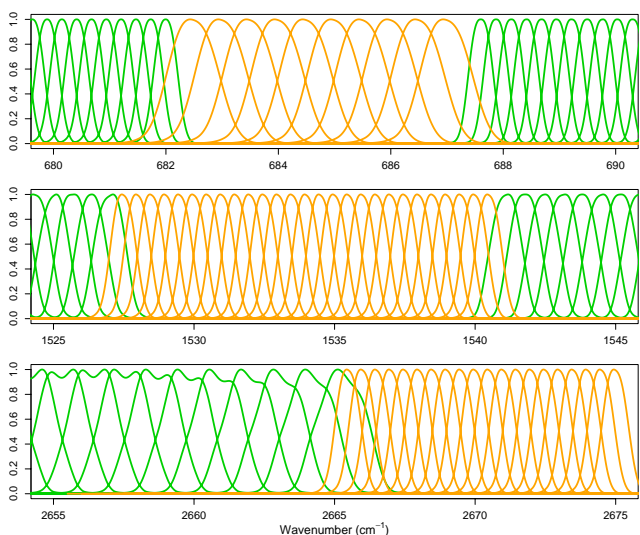


Figure 4: Examples of the SRFs of AIRS channels (green lines) and AIRS gap channels (orange lines). The SRFs of the AIRS channels are obtained from the Website of the Atmospheric Spectroscopy Laboratory (ASL) in the University of Maryland, Baltimore County (UMBC).

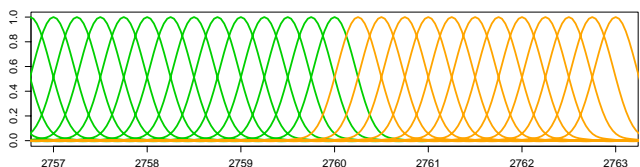


Figure 5: Example of the SRFs of IASI channels (green lines) and IASI gap channels (orange lines). The SRF of the IASI level 1c channels is obtained from the Website of the Sub Group for Radiative Transfer and Surface Property Models (RTSP) in the International TOVS Working Group (ITWG).

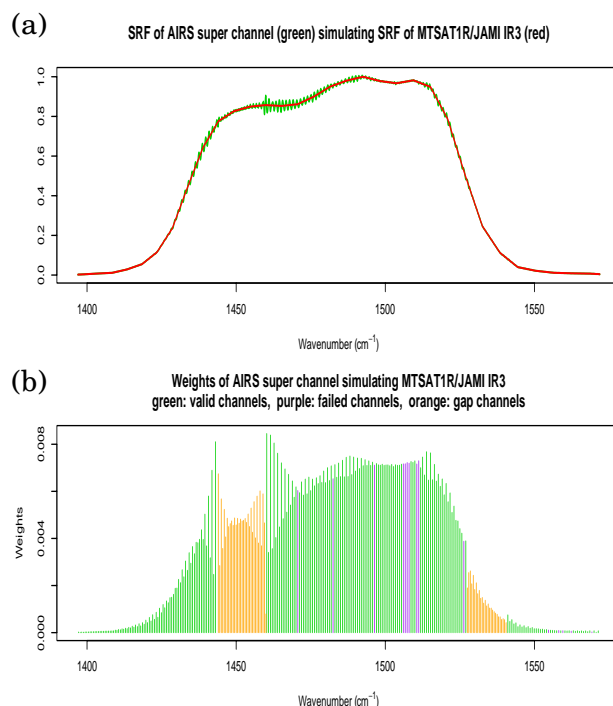


Figure 6: (a) shows SRFs of MTSAT-1R channel IR3 ($6.8 \mu\text{m}$) (red) and AIRS super channel (green). (b) shows weights of AIRS valid channels (green), AIRS failed channels (purple) and AIRS gap channels (orange) to construct the AIRS super channel in (a).

if the spectral information of the missing (failed and gap) channels is compensated for. This study introduces a spectral compensation method based on the spectral information with respect to eight atmospheric model profiles.

The radiances of the missing channels are calculated by regression analysis using radiative transfer simulated radiances with respect to the eight atmospheric model profiles as explanatory variables.

$$\log I_i^{\text{calc}} = c_0 + \sum_{k=1}^K c_k \log I_{i,k}^{\text{sim}}, \quad (3)$$

$(i = \text{hyper and gap channels})$

where I_i^{calc} is the calculated radiance of the hyper channel i , $I_{i,k}^{\text{sim}}$ is the simulated radiance of the hyper channel i with respect to the atmospheric model profile k , c_k ($k = 0, \dots, K$) are regression coefficients, and K is the number of the atmospheric model profiles. (3) introduces logarithm radiances as response and explanatory variables in order to increase fitting accuracy and avoid calculation of negative radiance.

The regression coefficients c_k are independent of the hyper channels, and are generated for each observing position of the hyper sounder. c_k are obtained by the least-square method applying a set of validly observed radiances I_i^{obs} in place of I_i^{calc} to (3),

$$\{c_k\} = \underset{i = \text{exist}(I_i^{\text{obs}})}{\text{argmin}} \sum \left\{ \log I_i^{\text{obs}} - \left(c_0 + \sum_k c_k \log I_{i,k}^{\text{sim}} \right) \right\}^2. \quad (4)$$

Once the regression coefficients c_k are computed, the radiances of the missing channels can be calculated by (3). It might be possible to apply the observed radiances of

all hyper channels to (4) to compute c_k and then calculate the radiances of all missing channels at once. However, this yields a large fitting error in practice. In intercalibration application, the coefficients c_k are computed for each broadband channel spectral region.

(3) and (4) use the simulated radiances $I_{i,k}^{\text{sim}}$. For the radiance simulation, this study uses the following eight atmospheric model profiles:

1. U.S. standard without cloud,
2. U.S. standard with cloud at 500 hPa altitude,
3. U.S. standard with cloud at 200 hPa altitude,
4. Tropic without cloud,
5. Tropic with cloud at 500 hPa altitude,
6. Tropic with cloud at 200 hPa altitude,
7. Mid-latitude summer without cloud,
8. Mid-latitude winter without cloud.

These profiles include not only clear weather conditions but also cloudy conditions because (3) should be applicable under any weather conditions. There is no high-latitude profile among the eight. In case of intercalibration between polar orbiting satellites examined over the polar regions, high latitude profiles should be implemented. However, the intercalibration for geostationary satellites examines over the Tropics and middle latitudes, and needs profiles there.

As for radiative transfer code, the line-by-line code LBLRTM (Clought et al., 1995) version 11.1 is used with the HITRAN2004 spectroscopy line parameter database (Rothman et al., 2003) including the AER updates version 2.0 (AER Web page). The emissivities of the surface and clouds are assumed to be one.

The benefit of this spectral compensation method is that it does not use radiative transfer computation in intercalibration operation. This not only speeds up the computation but also prevents super channel radiance computation from introducing biases contained in radiative transfer code and atmospheric state fields. In addition, the method is applicable to cloudy weather conditions, where it is very difficult to prepare atmospheric fields for radiative transfer simulation.

Figure 7 shows an example of the radiance calculation for the AIRS channels over the spectral range of MTSAT-1R channel IR3 (6.8 μm). The red boxes in Figure 7 (a) represent AIRS observed radiances I_i^{obs} over a cloud-free scene, and the black lines represent calculated radiances I_i^{calc} by (3). Simulated radiances with respect to the eight model profiles $I_{i,k}^{\text{sim}}$ are drawn by the colored lines. The sequence of the AIRS observed radiances varies widely because the observing scene is clear and the observed radiances are affected by strong and diverse water vapor absorption and emission over the IR3 band. Although the distribution of the AIRS observed radiances is complex, the computed radiances by (3) show good agreement with the observed ones.

Figure 7 (b) shows the residuals of the calculated values in Figure 7 (a) from the AIRS observations. Brightness temperature residuals are plotted instead of radiance residuals to ease the understanding of the magnitude of the residuals. The residuals are within the range of ± 1 K, and root mean square (RMS) of the residuals is 0.29 K. RMS of the radiance residuals is $0.075 \text{ mW} \cdot \text{m}^{-2} \cdot \text{sr}^{-1} \cdot \text{cm}$. The residuals are expected to represent the

accuracy of calculated radiances of the AIRS missing channels.

Figure 8 shows the same residuals as Figure 7, but for a scene containing clouds at the middle altitude. The AIRS observed radiances displayed by the red boxes in Figure 8 (a) show a smooth sequence with small down transitions. The red boxes on the smooth sequence show the radiances capturing emissions mainly from the top of the cloud. The red boxes on the down transitions show the radiances capturing emissions from both

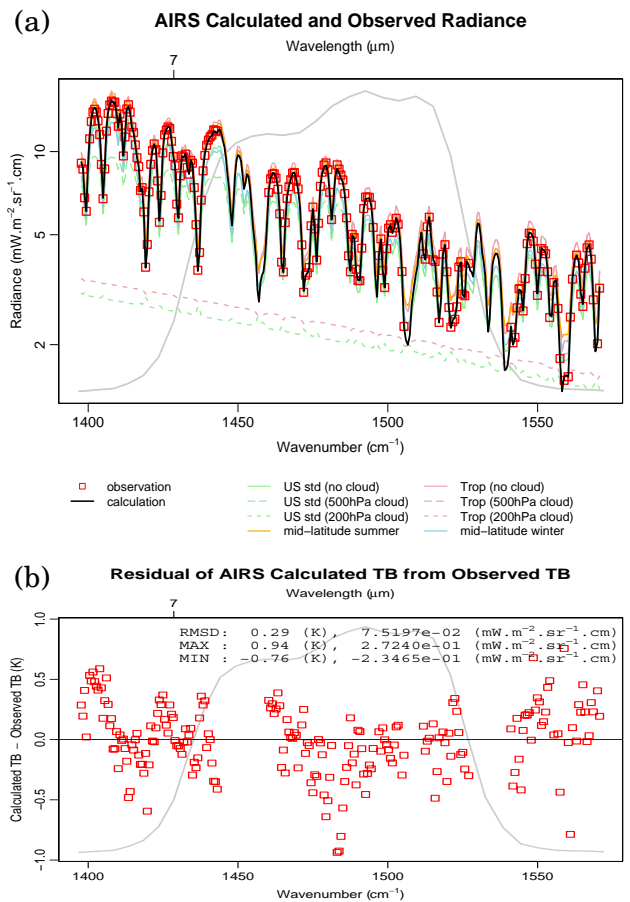


Figure 7: (a) shows an example of AIRS observed radiances (red boxes), calculated radiances (black lines) by (3) associated with the observations and simulated radiances (colored lines) with SRF of MTSAT-1R channel IR3 (6.8 μm) (gray line). The vertical axis is shown in log scale. (b) shows brightness temperature differences between the AIRS observations and calculations shown in (a).

the cloud and water vapor contained in the atmosphere above the cloud. In case of a scene affected by cloud and water vapor, calculated radiances by (3) (black lines) correspond considerably to the observed ones (red boxes).

Figure 8 (b) shows the residuals of the calculated brightness temperatures from the AIRS observed brightness temperatures. Even though brightness temperature sensitivity increases as radiance decreases over the infrared region, the RMS of the brightness temperature residuals is 0.23 K, which is smaller than that of the clear scene in Figure 7 (b). The RMS of the radiance residuals is 0.031 $mW \cdot m^{-2} \cdot sr^{-1} \cdot cm$, which is less than half that of the clear scene.

Figure 9 shows the same residuals as Figure 7, but for a scene dominated by thick clouds at the upper altitude. The very smooth sequence of the AIRS observed radiances (red boxes) in Figure 9 (a) indicates that AIRS captures the emission from the cloud mainly with very small effects of water vapor absorption and emission. In case of such an upper cloud scene, the calculated radiances by (3) (black lines) are well correlated to the observed ones (red boxes) as well as other scenes in Figure 7 (a) and Figure 8 (a). This good correlation is due to the use of the simulated radiances for the cloudy atmospheric model profiles in (3).

Figure 9 (b) shows the residuals of the calculated brightness temperatures from the

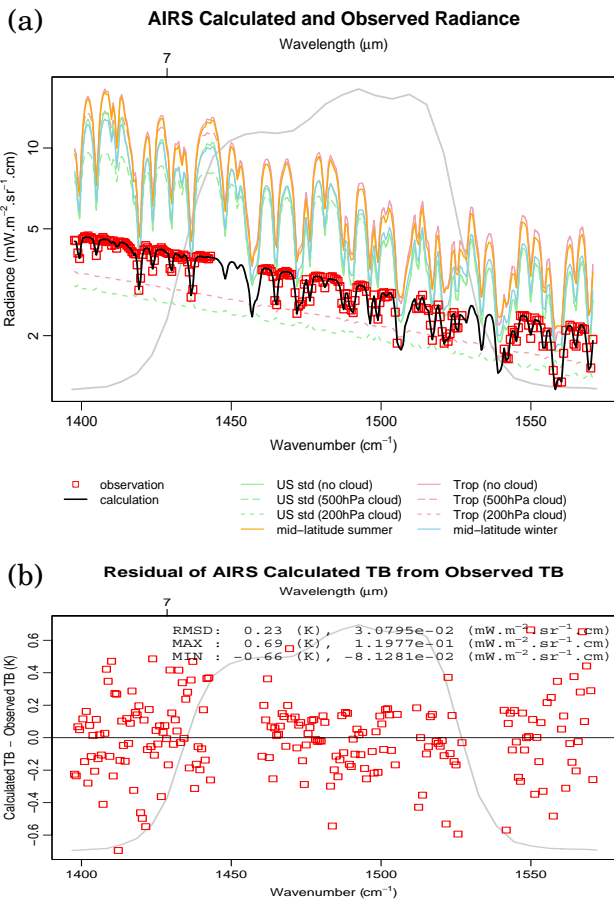


Figure 8: The same as Figure 7, but for a scene containing clouds at middle troposphere.

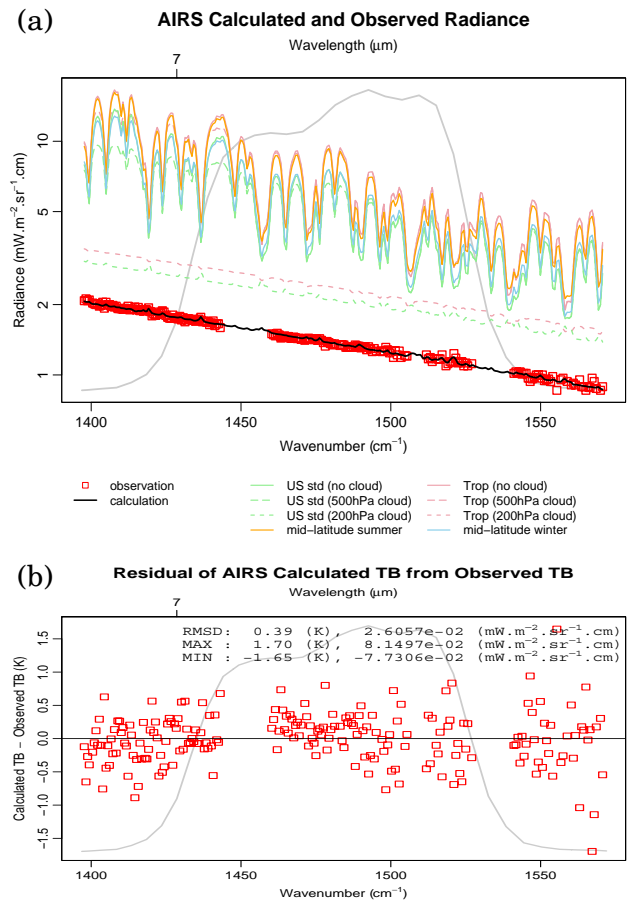


Figure 9: The same as Figure 7, but for a scene containing clouds at upper troposphere.

AIRS observed brightness temperatures. The RMS of the brightness temperature residuals is increased to 0.39 K because the brightness temperature sensitivity increases as radiance decreases. However, the RMS of the radiance residuals is $0.026 \text{ mW}\cdot\text{m}^{-2}\cdot\text{sr}^{-1}\cdot\text{cm}$, which is the smallest among the three examples.

Charts (c) and (d) of the figures in the Appendix show the same as Figure 7 (a) and (b), but for the spectral regions of other geostationary imager channels. The calculated radiances (black lines) by (3) also show good agreement with the observed ones (red boxes). This agreement is recognized even the spectral regions of the carbon dioxide absorption (Figure 21 and 32) and the ozone absorption (Figure 24).

2.4 Procedure to compute super channel radiance

The radiance of a super channel consisting of hyper channels to simulate a broadband channel is computed by (1) using hyper sounder observed radiances and the calculated radiances of hyper sounder missing (failed and gap) channels. Figure 10 shows off-line procedures to generate parameters necessary for the computation of AIRS/IASI super channel radiances to simulate the MTSAT-1R infrared channels. The weights w_i characterizing the super channels are generated by the constraint method (Tahara, 2007) referring to the SRFs of the broadband channels and the hyper channels including the gap channels. To calculate the radiances of the hyper sounder missing channels, the simulated radiances $I_{i,k}^{\text{sim}}$ of the hyper and gap channels with respect to the eight atmospheric model profiles should be also computed beforehand.

$I_{i,k}^{\text{sim}}$ are computed by integrating line-by-line simulated radiances associated with the SRFs of the hyper and gap channels.

In the intercalibration operation, super channel radiances are computed at the step displayed on the right side of Figure 1. Figure 11 shows the details of this step. After reading the super channel weights w_i and the simulated radiances $I_{i,k}^{\text{sim}}$, there are two loops for hyper sounder observing points and broadband channels. In the loops, the regression coefficients c_k are computed by (4) applying the hyper sounder observed radiances I_i^{obs} , which have already been read in the previous step shown in Figure 1, and the simulated radiances $I_{i,k}^{\text{sim}}$ within the spectral band of the particular broadband channel. Then, the radiances of the missing channels I_i^{calc} are calculated by (3) using the computed coefficients c_k and the simulated radiances $I_{i,k}^{\text{sim}}$ of the missing channels. Finally, the radiance of the super channel I_s to simulate the broadband channel radiance at the hyper

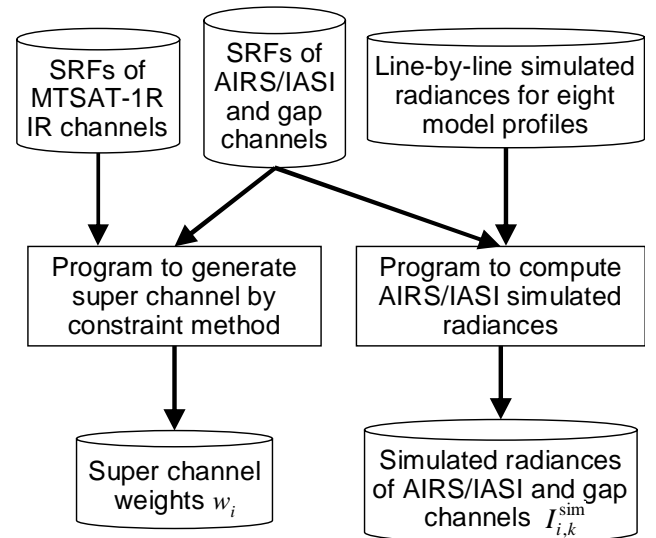


Figure 10: Flow chart to generate parameters used by the computation of super channel radiance.

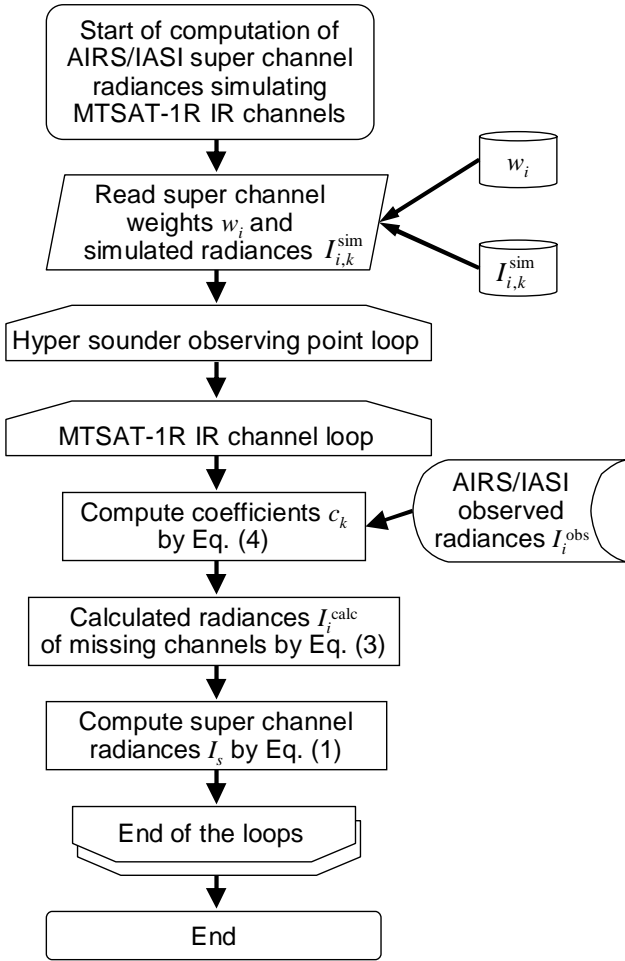


Figure 11: Flow chart to compute AIRS/IASI super channel radiances simulating the MTSAT-1R infrared channels.

sounder observing point is computed by (1) using the hyper sounder observed radiances I_i^{obs} and the calculated radiances I_i^{calc} of the missing channels.

3 Validation

Figure 2 shows SRF of the super channel simulating MTSAT-1R channel IR3 (6.8 μm) from the AIRS channels excluding the AIRS failed channels and the AIRS spectral gaps. Using this super channel, the SRF departure is expected to cause systematic bias in the radiance of the super channel.

Meanwhile, Figure 7 (b), 8 (b) and 9 (b)

show examples of residuals of the calculated brightness temperatures from the AIRS observed brightness temperatures. These residuals represent radiance calculation accuracy for the AIRS missing channels. However, the impact using the calculated radiances on super channel radiance computation is not clear from the examples.

To evaluate the impacts of the AIRS failed channels and the AIRS spectral gaps on the AIRS super channel, the IASI super channel is used to simulate the AIRS channel. Since IASI fully covers the IR3 spectral band as mentioned in Section 2.2, the super channel consisting of only IASI channels S^{all} , whose SRF is shown by the red lines in Figure 12, can be assumed to be true under the condition that IASI observation error is neglected. Then, two IASI super channels are evaluated.

S^{gap} : The same super channel as S^{all} , but excluding IASI channels corresponding to the AIRS missing channels.

S^{calc} : The same super channel as S^{all} , but spectral compensation is applied by using calculated radiances for the IASI channels excluded in S^{gap} .

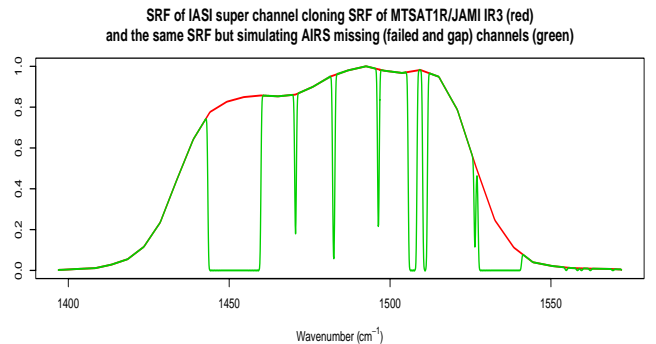


Figure 12: SRFs of MTSAT-1R channel IR3 (6.8 μm) (red) and the IASI super channel generated by excluding the IASI channels corresponding to the AIRS missing (failed and gap) channels (green).

As mentioned in Section 2.2, 26 AIRS channels out of 293 are failed over the IR3 spectral band, and 60 gap channels are inserted. To simulate these AIRS missing channels, 161 IASI channels out of 700 are treated as failed. The green lines in Figure 12 show SRF of the super channel S^{gap} . The SRF is similar to that of the AIRS super channel shown by the green lines in Figure 2.

Figure 13 (a) shows brightness temperature residuals of the super channel S^{gap} from S^{all} . The residuals originate from the SRF difference shown in Figure 12. Without the IASI channels corresponding to the AIRS missing channels, systematic bias is recognized, and the mean residuals with respect to brightness temperature vary from about -0.35 K at 200 K to 0.2 K at 260 K. Since the required specification of IR3 calibration accuracy is less than 0.10 K at 220 K and 0.21 K at 300 K, such systematic residuals may prevent intercalibration using the AIRS super channel.

Figure 13 (b) shows the same residuals as (a), but those of the super channel S^{calc} from S^{all} . The impact of the compensation for the AIRS missing channels on the super channel can be evaluated. The residuals are significantly decreased from Figure 13 (a). The absolute values of the mean residuals with respect to brightness temperature are decreased at most 0.05 K at 240 K. The distribution of the residuals is also reduced apparently. Most of the residuals are within ± 0.1 K, and smaller than the required specification of the IR3 calibration accuracy. The reduction of the residual distribution indicates that the calculated radiances substantially represent exiting radiances at the top of the atmosphere.

These results clearly show that the spectral compensation by using calculated radiances for the AIRS missing channels significantly improves the intercalibration using the AIRS super channel.

Charts (f) and (g) of the figures in the Appendix show the same residuals as Figure 13 (a) and (b), but for super channels to

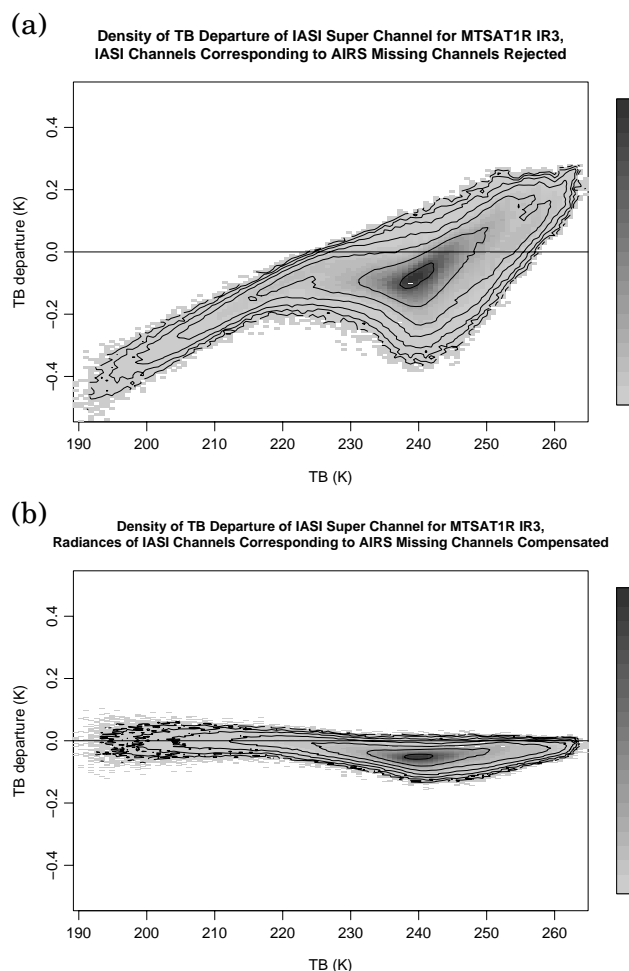


Figure 13: (a) shows the density plot of brightness temperature residuals of an IASI super channel for MTSAT-1R channel IR3 ($6.8 \mu m$) excluding IASI channels corresponding to AIRS missing (failed and gap) channels from the same super channel but using all IASI channels. (b) shows the same density plot as (a), but the residuals of an IASI super channel using calculated radiances for the excluded IASI channels in (a). The contour lines are drawn by the intervals of logarithm scale. One month IASI data in August 2008 over the west Pacific region are used.

simulate other geostationary imager channels. Comparing Charts (f) and (g) in the Appendix, the mean residuals with respect to brightness temperature are decreased by using this compensation technique for all the imager channels. The variations of the residuals are also decreased for the imager channels except for the MTSAT-1R channel IR4 ($3.8 \mu\text{m}$) in Figure 20 and METEOSAT-8 $8.7 \mu\text{m}$ channel in Figure 25, both of which need spectrally wide compensation.

4 Application to intercalibration of MTSAT-1R infrared channels

The intercalibration of the MTSAT channels with AIRS is examined. Two-month data from 1st May to 31st June 2008 are compared. Daytime data are compared for the MTSAT-1R IR1 ($10.8 \mu\text{m}$), IR2 ($12.0 \mu\text{m}$) and IR3 ($6.8 \mu\text{m}$) because the trend of the MTSAT-1R calibration might be shifted around midnight due to solar heating influence on the sensor, and the shift should be excluded in the discussion of the intercalibration methodology. Only nighttime data are compared for the channel IR4 ($3.8 \mu\text{m}$) because this channel is affected by the sun. To match-up observed data between MTSAT-1R and AIRS, an algorithm proposed by the GSICS Research Working Group (GRWG) is used (GSICS Coordination Center).

Figure 14 (a) shows radiance differences between IR3 and the AIRS super channel, to which the spectral compensation for the AIRS missing channels is applied. The points plotted higher than the horizontal zero line indicate that the IR3 radiances are higher than the AIRS ones. Positive biases from many IR3 radiances are recognized, and the biases

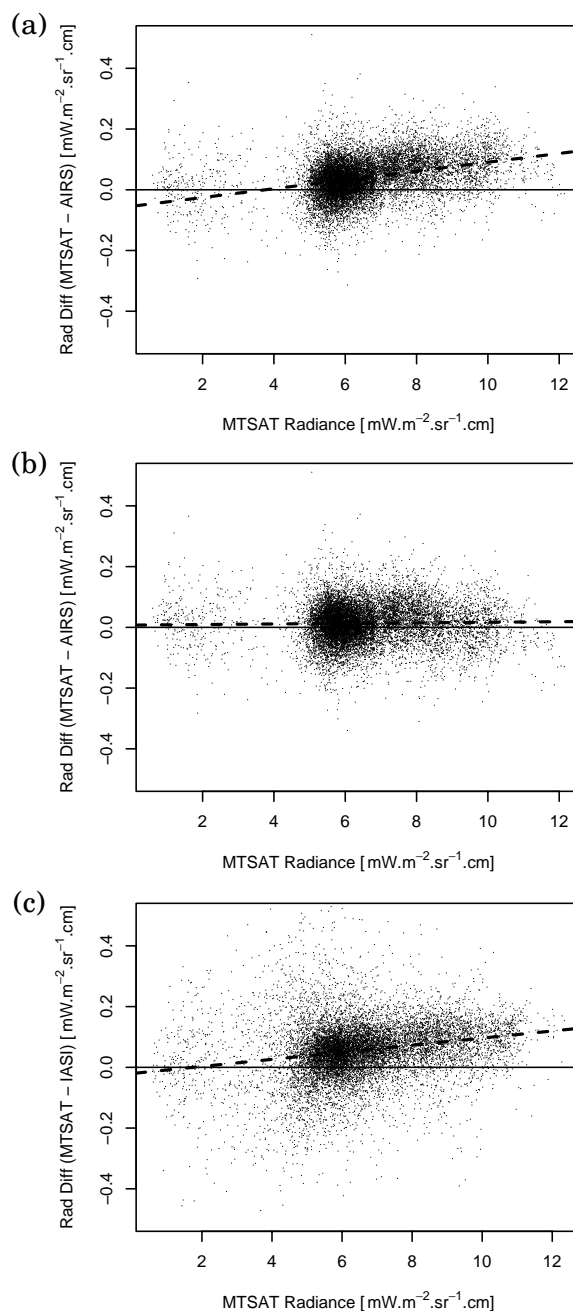


Figure 14: (a): Radiance differences between MTSAT-1R channel IR3 ($6.8 \mu\text{m}$) and AIRS super channel, whose spectra are compensated by using calculated radiances for AIRS failed and gap channels. (b): The same chart as (a), but without using the calculated radiances. (c): The same chart as (a), but the differences between IR3 and IASI super channel. The dashed thick lines correspond to linear regression lines computed in radiance space. Daytime data for 1 May and 30 June 2008 are compared.

increase as radiance increases.

Figure 14 (b) shows the same differences as (a), but the AIRS super channel is generated from the AIRS channels excluding the AIRS missing channels instead of applying the compensation. The points are distributed around the horizontal zero line. Compared with Figure 14 (a), the compensation seems to degrade the AIRS super channel radiance computation.

The dashed thick lines in Figure 14 (a) and (b) represent linear regression lines. It is true that the spectral compensation increases the mean difference between IR3 and the AIRS super channel. However, the residual standard errors of the linear regressions are $0.0613 \text{ mW} \cdot \text{m}^{-2} \cdot \text{sr}^{-1} \cdot \text{cm}$ for Figure 14 (a) and $0.0644 \text{ mW} \cdot \text{m}^{-2} \cdot \text{sr}^{-1} \cdot \text{cm}$ for (b), respectively. There are three reasons expected to cause the standard errors: variation error involved in observed radiances, observing condition inconsistency between collocated data and variation error in the computed AIRS super channel radiances. Since Figure 14 (a) and (b) display the comparisons using the same IR3-AIRS collocation data, the difference of the residual standard errors between the two charts represents the variation error involved in the AIRS super channel radiances. Therefore, the spectral compensation contributes to increasing correlation between the IR3 radiances and the AIRS super channel radiances.

Figure 14 (c) shows radiance differences between IR3 and the IASI super channel. There are no IASI missing channels contained in the IASI super channel. The plot is very similar to that in Figure 14 (a). Positive bias and a

Table 1: Brightness temperature differences of MTSAT-1R channel IR3 ($6.8 \mu\text{m}$) from an AIRS super channel with spectral compensation, the same super channel but without spectral compensation and an IASI super channel at reference brightness temperatures of 220 K, 250 K and 300 K. The differences are computed associated with linear regression analyses examined on radiance space.

Reference temperature [K]	220	250	300
AIRS (compensated) [K]	-0.18	+0.22	+0.54
AIRS (not compensated) [K]	+0.09	+0.06	+0.05
IASI [K]	+0.07	+0.27	+0.47

right-up trend are recognized.

Table 1 shows the brightness temperature differences of IR3 from the AIRS and IASI super channels at reference brightness temperatures of 220 K, 250 K and 300 K. The differences are computed associated with the regression analyses shown by the dashed thick lines in Figure 14. The differences from the AIRS super channel without the spectral compensation are departed from those from the IASI super channel. The discrepancies of the brightness temperature differences against the AIRS and IASI super channels are 0.21 K (= $0.27 \text{ K} - 0.06 \text{ K}$) at 250 K and 0.42 K (= $0.47 \text{ K} - 0.05 \text{ K}$) at 300 K. The discrepancies are decreased to 0.05 K at 250 K and 0.07 K at 300 K by applying the spectral compensation to the AIRS super channel. Assuming that both IASI and AIRS calibrations are accurate, the 0.07 K discrepancy at 300 K mainly originates from the spectral compensation error. However, this value is smaller than 0.21 K at 300 K, which is the calibration accuracy requirement for the MTSAT-1R infrared channel. The 0.25 K discrepancy at 220 K is recognized even though the spectral compensation is applied. The reason for this is

not clear. However, comparison over such a low brightness temperature region is difficult due to the small number of samples and increase of brightness temperature sensitivity against radiance.

These results indicate that the AIRS super channel simulating IR3 can be made comparable with that of the IASI with the help of spectral compensation. It is thought that the biases shown in Figure 14 (a) and (c) mainly originate from IR3 calibration bias.

Figures 15 and 16 show the same radiance differences as Figure 14, but for MTSAT-1R channel IR1 (10.8 μm) and IR2 (12.0 μm), respectively. The distribution of points over the lower brightness temperature region is large because conditions for collocating data between MTSAT-1R and AIRS/IASI are relaxed to increase the number of samples over a brightness temperature range smaller than 275 K. Comparing the charts between Figure 15 (a) and (b) and between Figure 16 (a) and (b), the impact of the spectral compensation on the AIRS super channel is not clear. Such a small impact is expected in validation using the IASI super channel as shown in Figure 18 (f) and (g) and Figure 19 (f) and (g) in the Appendix.

Tables 2 and 3 are the same as Table 1, but for IR1 and IR2, respectively. Both tables indicate that the brightness temperature differences of IR1 and IR2 from the AIRS super channels at 300 K come closer to those from the IASI super channels by applying the spectral compensation method. A small improvement by using the spectral compensation is recognized.

Figure 17 is the same as Figure 14, but for MTSAT-1R channel IR4 (3.8 μm). Figure 17

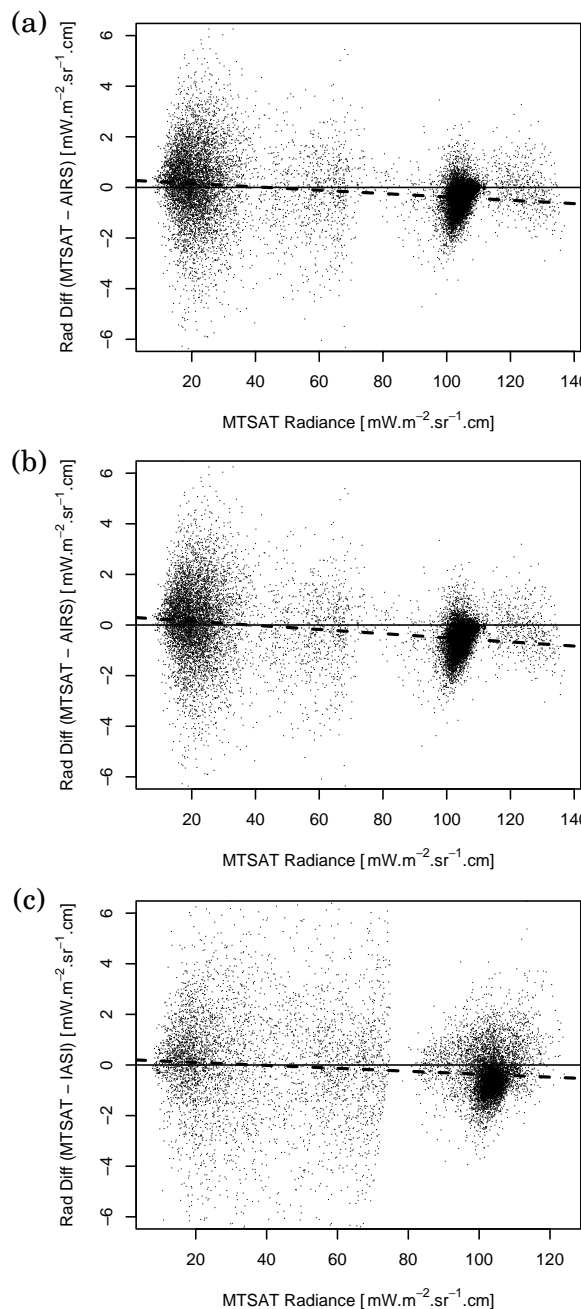


Figure 15: The same figure as Figure 14, but for MTSAT-1R channel IR1 (10.8 μm).

Table 2: The same table as Table 1, but for MTSAT-1R channel IR1 (10.8 μm).

Reference temperature [K]	220	250	300
AIRS (compensated) [K]	+0.23	-0.02	-0.27
AIRS (not compensated) [K]	+0.22	-0.06	-0.36
IASI [K]	+0.14	-0.05	-0.26

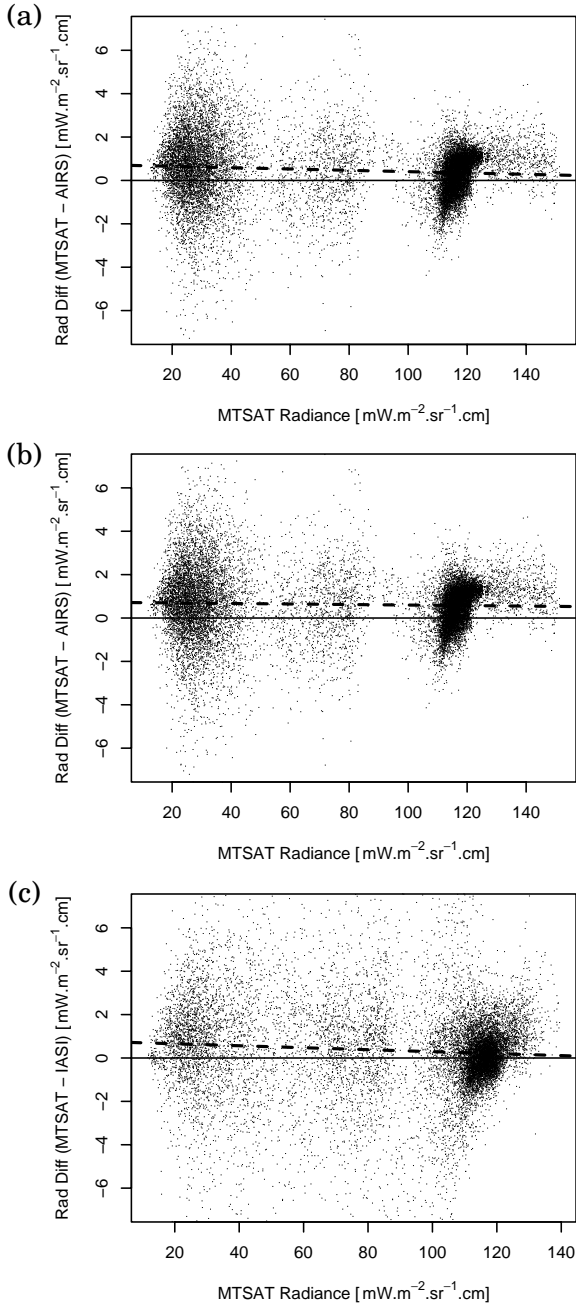


Figure 16: The same figure as Figure 14, but for MTSAT-1R channel IR2 (12.0 μm).

Table 3: The same table as Table 1, but for MTSAT-1R channel IR2 (12.0 μm).

Reference temperature [K]	220	250	300
AIRS (compensated) [K]	+0.84	+0.48	+0.18
AIRS (not compensated) [K]	+0.93	+0.59	+0.32
IASI [K]	+0.83	+0.44	+0.10

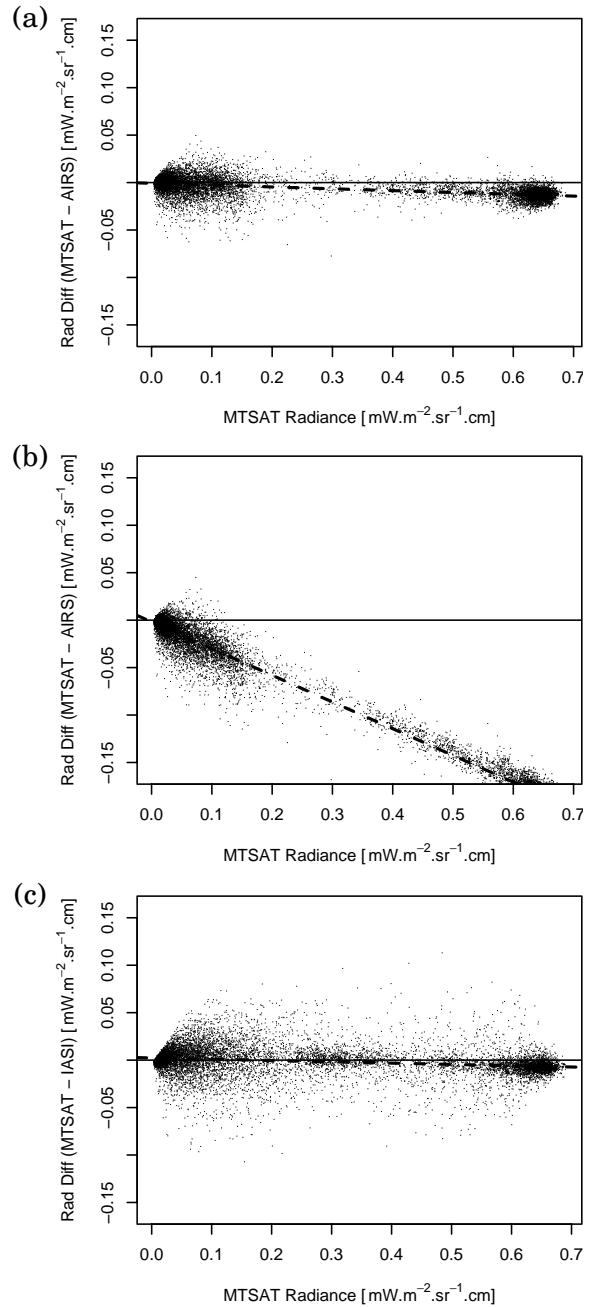


Figure 17: The same figure as Figure 14, but for nighttime intercalibration of MTSAT-1R channel IR4 (3.8 μm).

Table 4: The same table as Table 1, but for nighttime intercalibration of MTSAT-1R channel IR4 (3.8 μm).

Reference temperature [K]	220	250	300
AIRS (compensated) [K]	-1.55	-0.54	-0.48
AIRS (not compensated) [K]	-5.63	-4.62	-6.09
IASI [K]	+4.47	+0.45	-0.25

(b) shows large differences between IR4 and the AIRS super channel excluding the AIRS missing channels. Since AIRS only covers half of the IR4 spectral band, the spectral compensation is crucial for the intercalibration as expected by the validation using the IASI super channel shown in Figure 20 (f) and (g) in the Appendix. Figure 17 (a) shows a small negative bias of IR4 radiance against AIRS radiance over the larger radiance region, which is similarly recognized in the radiance comparison between IR4 and IASI shown in Figure 17 (c).

Table 4 is the same as Table 1, but for IR4. Since brightness temperature sensitivity against radiance increases intensely as radiance decreases on the shorter wavelength infrared region, large brightness temperature differences are recognized at 220 K and 250 K. The brightness temperature differences of IR4 from the AIRS super channel at 300 K show significant improvement with the spectral compensation as recognized in Figure 17 (a). The spectral compensation is important and effective for the comparison between IR4 and AIRS.

Although an improvement is recognized, there is a 0.23 K discrepancy at 300 K between AIRS comparison and IASI comparison. This discrepancy is larger than 0.01 K for IR1 (Table 2), 0.08 K for IR2 (Table 3) and 0.07 K for IR3 (Table 1). There are two expected reasons. One originates from wide spectral range compensation examined in the spectral compensation to cover the IR4 band. Such spectrally wide compensation degrades the accuracy of the AIRS super channel simulating IR4. Another originates from the variation of

the IR4 calibration around midnight. Since IR4 is a solar-affected channel, the comparison is examined by using nighttime data. The local observation time of IASI at night is around 09:30 pm, whereas that of AIRS is around 01:30 am. If there is some variation on the IR4 calibration around midnight, inconsistency would be expected between the IR4-AIRS and IR4-IASI comparisons.

5 Summary and plan

Tahara (2007) introduces a super channel for intercalibration between a broadband channel like an imager channel on a geostationary satellite and a high spectral resolution sounder (hyper sounder). The super channel is generated by the *constraint method* combining the channels of the hyper sounder (hyper channels). The method compares the data of the two channels narrowing their spectral differences in case the hyper sounder fully covers the spectral range of the broadband channel. However, if there are failed channels, spectral gaps and shortages in the hyper sounder, accuracy for the super channel to simulate the broadband channel degrades. To compensate for the spectral gaps and shortages contained in the hyper sounder, a new approach is proposed.

First, virtual channels named *gap channels* are introduced to fill the spectral gaps and shortages. Using the gap channels in addition to the hyper channels including failed channels, the super channel can be generated to have a spectral response nearly the same as that of the geostationary channel. The observed information of the geostationary channel can be simulated by using the super channel if the

spectral information of the missing (failed and gap) channels are compensated for. Second, this study introduces a spectral compensation method based on the spectral information with respect to eight atmospheric model profiles. The radiances of the missing channels are calculated by regression analysis using the beforehand radiative transfer simulated radiances with respect to the atmospheric model profiles including clear and cloudy weather conditions over the Tropics and mid latitudes. The regression coefficients are computed by applying validly observed radiances of the hyper channels to the response variable. Finally, a super channel radiance is computed by using the hyper sounder observed radiances in addition to the calculated ones for the missing channels.

The advantage of this spectral compensation method is that it does not use radiative transfer computation and numerical weather prediction fields in operation. This advantage enables it not only to compute super channel radiance fast, but also to prevent super channel radiance computation from introducing systematic biases originating from numerical weather prediction fields and radiative transfer simulation. In addition, this method is applicable to cloudy weather conditions, where it is very difficult to prepare atmospheric fields for radiative transfer simulation.

To validate the compensation technique, the AIRS missing (failed and gap) channels are simulated by IASI. The super channel using the calculated radiances of the IASI channels corresponding to the AIRS missing channels shows apparently better results than the same super channel excluding the IASI channels

corresponding to the AIRS missing channels.

The two-month intercalibration of MTSAT-1R channel IR3 (6.8 μm) against the AIRS super channel using the spectral compensation method shows a good agreement with that against the IASI super channel. This fact indicates that the spectral compensation is effective for this intercalibration. A small improvement of the spectral compensation is also recognized in the intercalibration of IR1 (10.8 μm) and IR2 (12.0 μm) against AIRS. With respect to the intercalibration of IR4 (3.8 μm) against AIRS, the spectral compensation is crucial because AIRS covers only half of the IR4 spectral band.

Although the spectral compensation technique is effective, degradation is recognized in cases where the spectral range to be compensated is wide. This is one of the causes of inconsistency between the IR4-AIRS comparison and that of IR4-IASI. Further investigation is planned to improve the spectral compensation method for the case of such wide spectral compensation.

Acknowledgments

The authors wish to express their thanks to the two anonymous reviewers for their helpful comments and suggestions, which led to a significant improvement of the earlier manuscript.

References

Clough, S. A., and M. J. Iacono, 1995: Line-by-line calculations of atmospheric fluxes and cooling rates II: Application to carbon dioxide, ozone, methane, nitrous oxide, and the halocarbons. *J. Geophys. Res.*,

100. 16519-16535.

Gunshor, M. M., T. J. Schmit, W. P. Menzel, and D. C. Tobin, 2006: Intercalibration of the newest geostationary imagers via high spectral resolution AIRS data. Conference on Satellite Meteorology and Oceanography, 14th, Atlanta, GA, January 29-February 2, 2006 (preprints). Boston, MA, American Meteorological Society, 2006, Paper P6.13.

Rothman et al., 2003: The HITRAN molecular spectroscopic database: edition of 2000 including updates through 2001, Journal of Quantitative Spectroscopy and Radiative Transfer. vol. 82, 5-44.

Tahara, Yoshihiko, 2008: New Approach to Intercalibration Using High Spectral Resolution Sounder. Meteorological Satellite Center Technical Note, No. 50, 1-14.

Tobin, D. C., H. E. Revercomb, C. C. Moeller, and T. Pagano, 2006: Use of Atmospheric Infrared Sounder high-spectral resolution spectra to assess the calibration of Moderate resolution Imaging Spectroradiometer on EOS Aqua, J. Geophys. Res., 111, D09S05, doi:10.1029/2005JD006 095.

http://mscweb.kishou.go.jp/monitoring/mtsats_monit.html

National Aeronautics and Space Administration (NASA): Goddard Earth Sciences (GES) Data and Information Services Center (DISC).
<http://daac.gsfc.nasa.gov/>

National Aeronautics and Space Administration (NASA), Jet Propulsion Laboratory (JPL): Atmospheric Infrared Sounder (AIRS).
<http://www-air.jpl.nasa.gov/>

Sub Group for Radiative Transfer and Surface Property Models (RTSP), International TOVS Working Group (ITWG): Satellite instrument characteristics for radiative transfer modeling and satellite data assimilation.
<http://cimss.ssec.wisc.edu/itwg/groups/rtwg/instrument.html>

University of Maryland, Baltimore County (UMBC), Atmospheric Spectroscopy Laboratory (ASL): Atmospheric Infrared Sounder (AIRS).
<http://asl.umbc.edu/pub/airs/airs.html>

Web pages

Atmospheric and Environmental Research (AER), Inc.: AER's Radiative Transfer Working Group.
<http://rtweb.aer.com/main.html>

GSICS Coordination Center.
<http://www.star.nesdis.noaa.gov/smcd/spb/calibration/icvs/GSICS/>

Meteorological Satellite Center (MSC): Monitoring of MTSAT-1R Navigation and Calibration.

APPENDIX

Super channels for MTSAT-1R, METEOSAT-8 and GOES-12

GSICS is an international project for geostationary satellite operation centers to examine intercalibration between imager channels on geostationary satellites and hyper sounders. In order to provide uniform quality information from the intercalibration, the comparison method used among the centers should be the same. Since the object of the spectral compensation method proposed by this report is to be used in the GSICS project, the infrared channels of MTSAT-1R, METEOSAT-8 and GOES-12 are reviewed.

Chart (a) in Figure 18 to 34 shows the SRF (green lines) of a super channel of AIRS or IASI. The SRF lines are well correlated with those of a simulated imager channel (red lines). Chart (b) shows the weights of the hyper channels to generate the super channel. The green, purple and orange lines represent the weights of the AIRS/IASI valid, failed and gap channels, respectively.

Chart (c) shows an example of calculated radiances (black lines) by (3) over a cloud-free scene from hyper channel observations (red boxes) by referring to the simulated radiances for the eight model profiles (colored lines). It is recognized that the calculated radiances are well correlated with the observed ones for all bands of the geostationary channels of infrared window, water vapor absorption, carbon dioxide absorption and ozone absorption. Chart (d) shows brightness temperature residuals associated with the differences between the calculated and observed radiances.

Chart (e) shows SRF as in Chart (a), but the

SRF of the AIRS super channel generated by excluding AIRS failed and gap channels.

Chart (f) shows the accuracy of the AIRS super channel excluding the AIRS missing (failed and gap) channels, whose SRF is shown by the green lines in Chart (e). Chart (g) is the same as Chart (f), but for the AIRS super channel where the spectral compensation is applied. The accuracy is computed by using IASI simulating the AIRS super channels as examined in Section 3. Comparing the charts between (f) and (g), the averages of the brightness temperature residuals in (g) are smaller than those in (f) for all geostationary channels. In particular, the improvement is very large for the cases of large SRF differences recognized in Chart (e).

There are no charts (e), (f) and (g) in Figure 33 and 34 because there is no other hyper sounder having wider spectral coverage than IASI, and the validation examined in Section 3 cannot be performed.

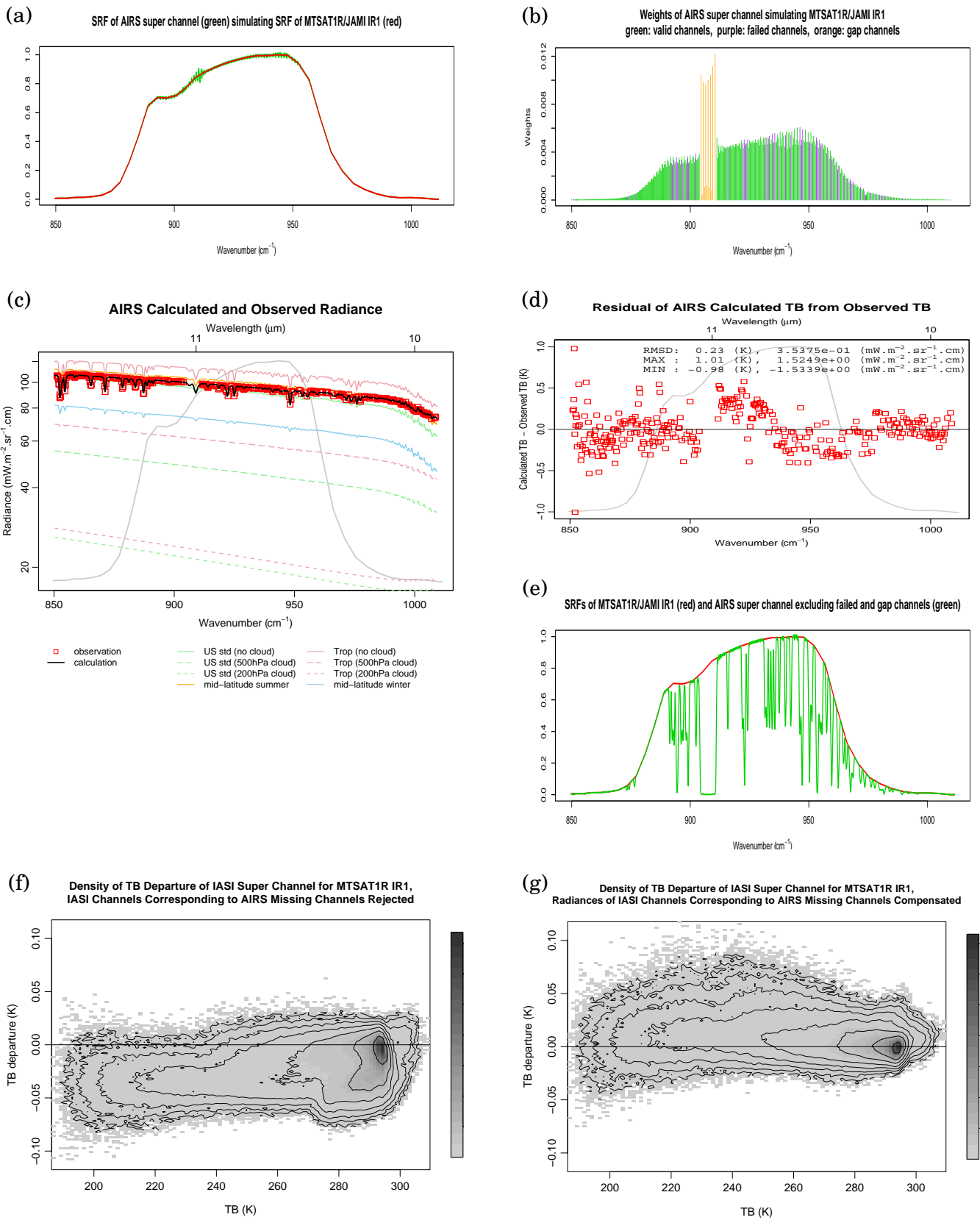


Figure 18: AIRS super channel simulating MTSAT-1R channel IR1 (10.8 μm). The explanations of the charts are written in the Appendix body text.

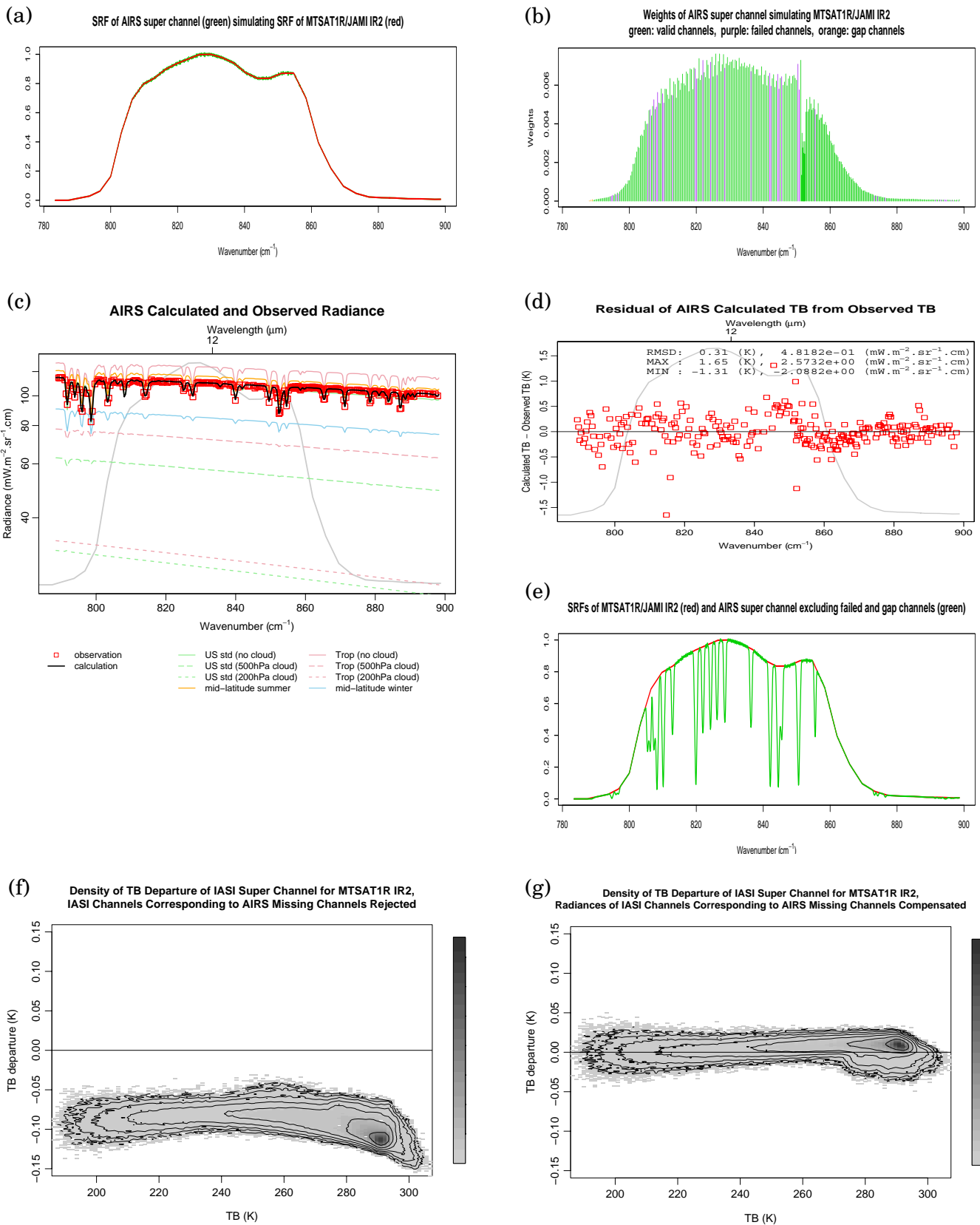


Figure 19: AIRS super channel simulating MTSAT-1R channel IR2 ($12.0\ \mu\text{m}$). The explanations of the charts are written in the Appendix body text.

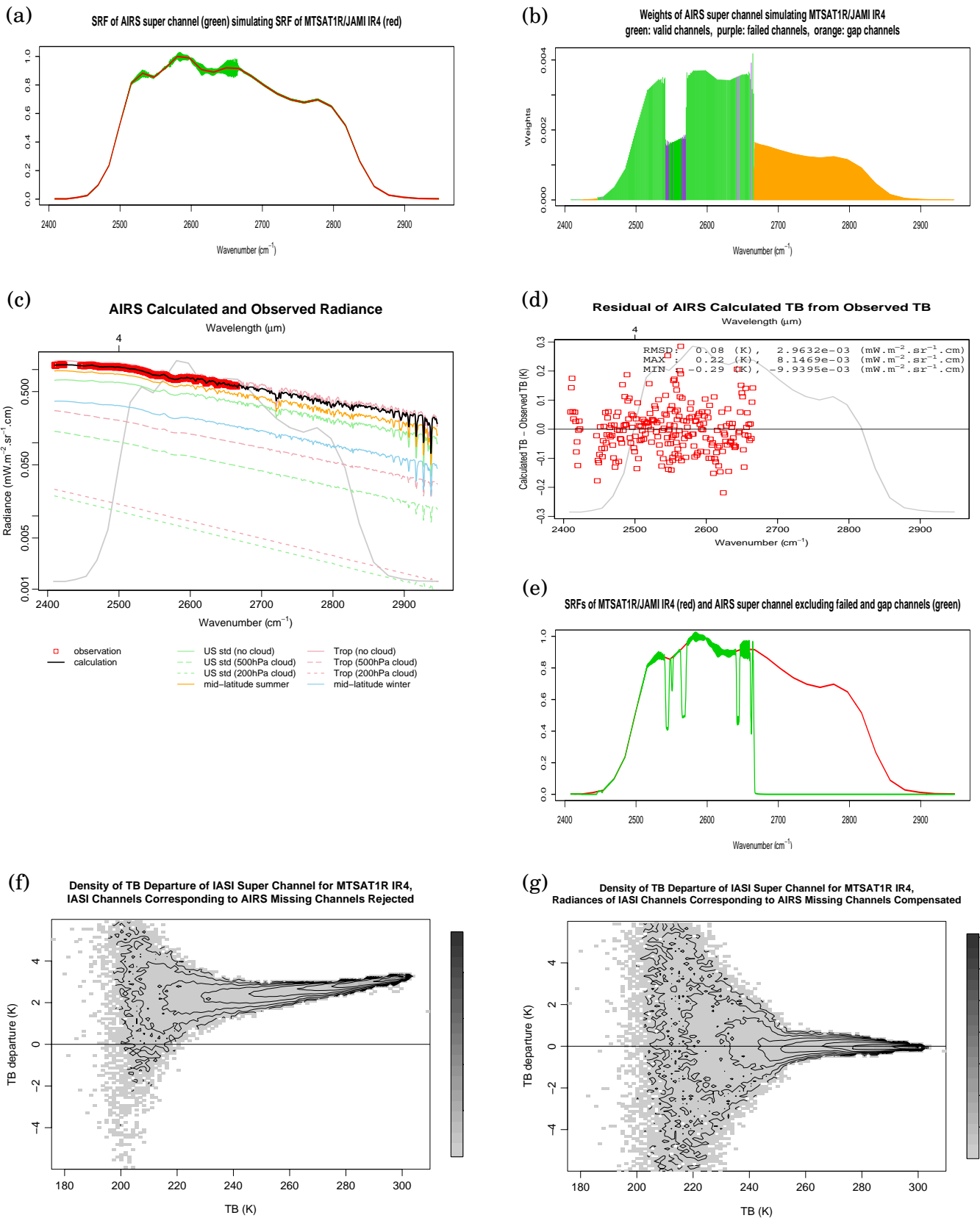


Figure 20: AIRS super channel simulating MTSAT-1R channel IR4 ($3.8 \mu\text{m}$). The explanations of the charts are written in the Appendix body text.

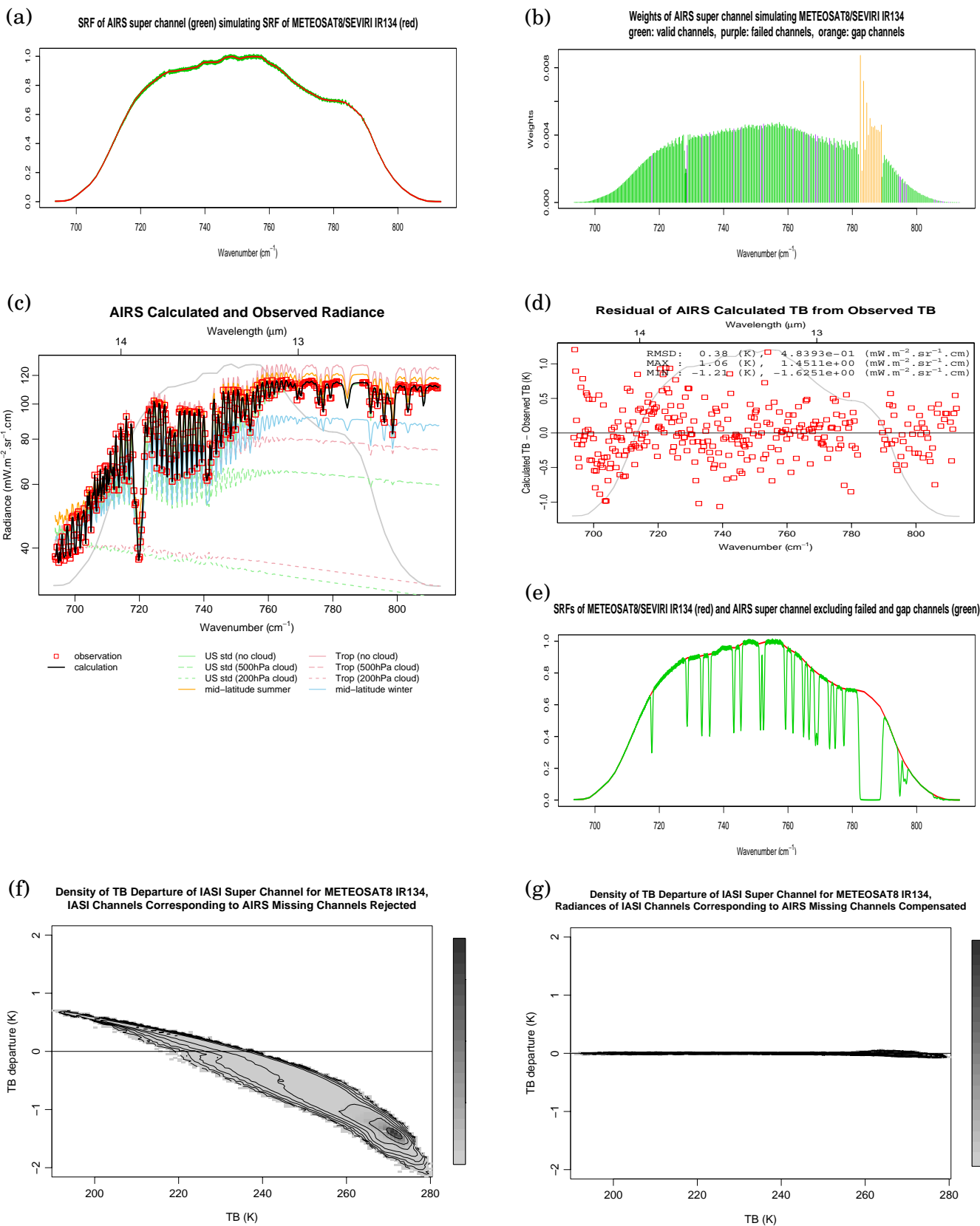


Figure 21: AIRS super channel simulating METEOSAT-8 13.4 μm channel. The explanations of the charts are written in the Appendix body text.

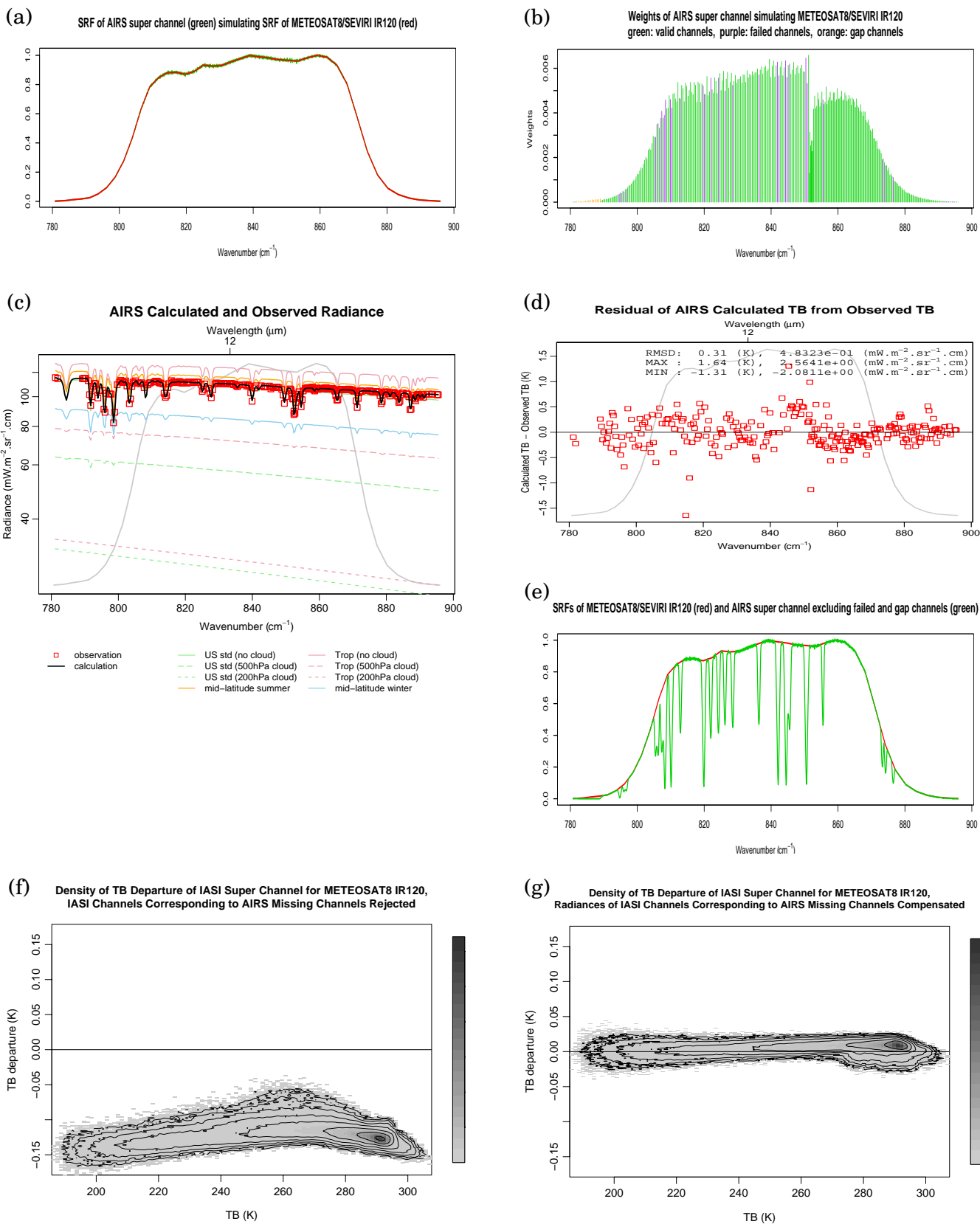


Figure 22: AIRS super channel simulating METEOSAT-8 12.0 μm channel. The explanations of the charts are written in the Appendix body text.

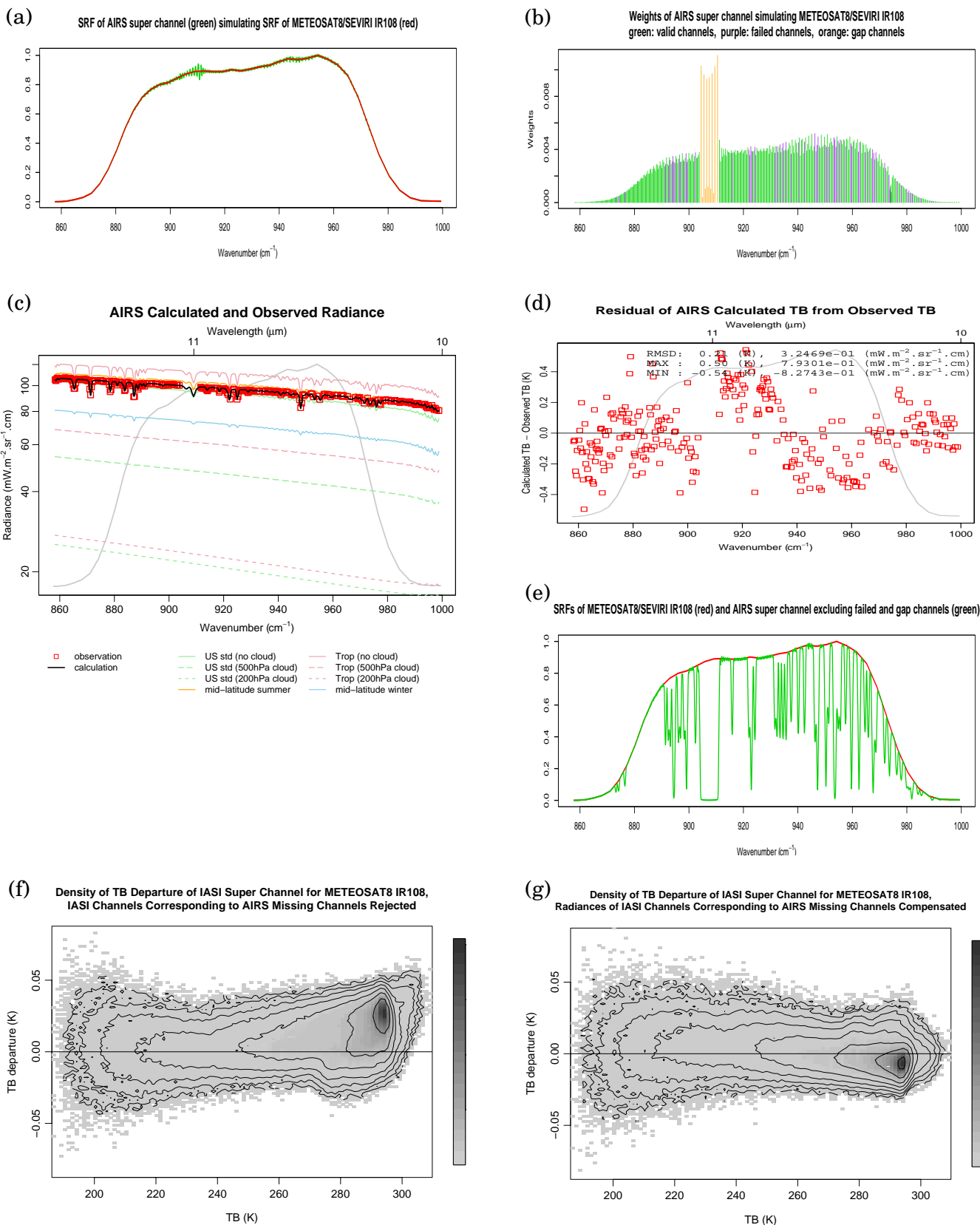


Figure 23: AIRS super channel simulating METEOSAT-8 10.8 μm channel. The explanations of the charts are written in the Appendix body text.

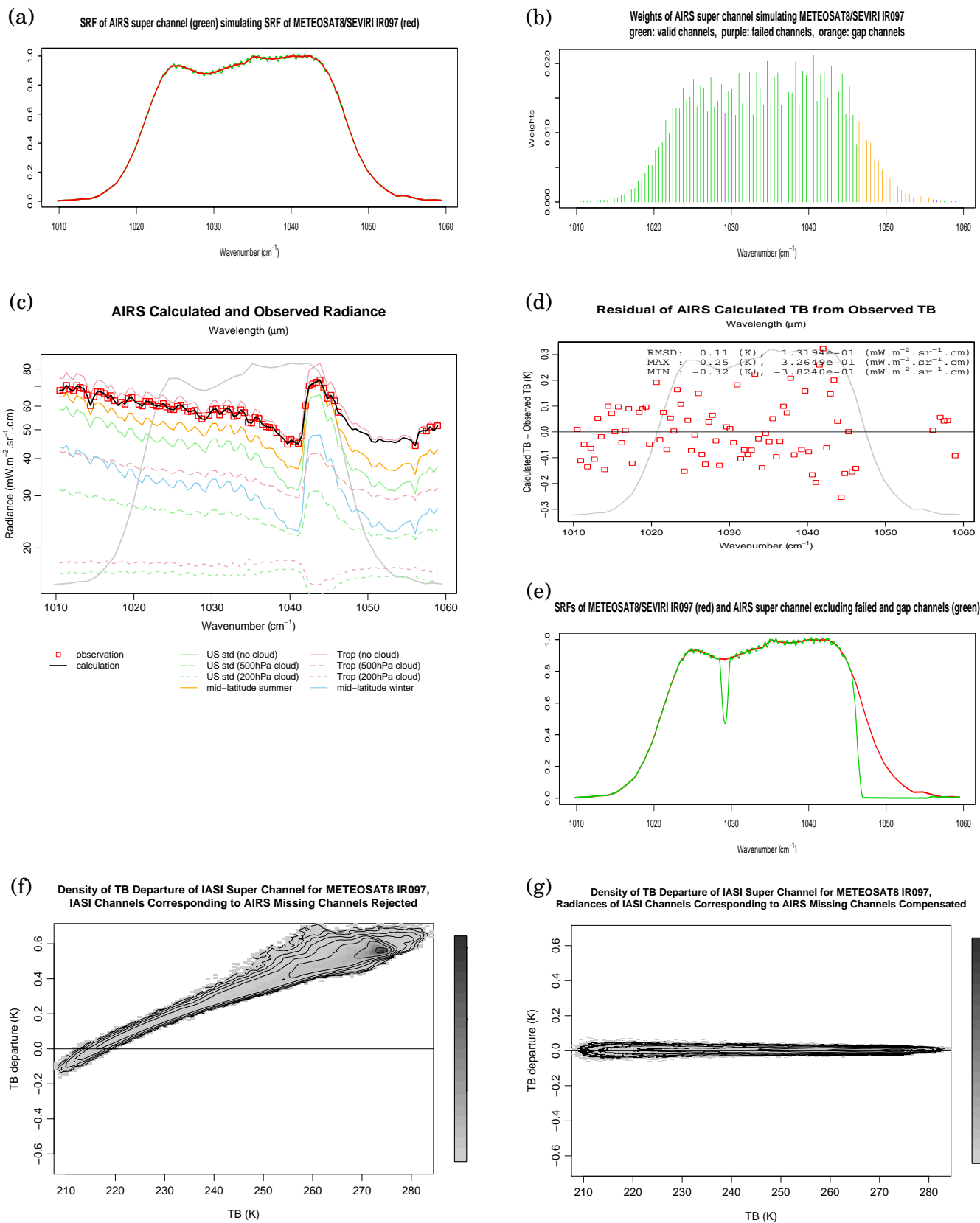


Figure 24: AIRS super channel simulating METEOSAT-8 9.7 μm channel. The explanations of the charts are written in the Appendix body text.

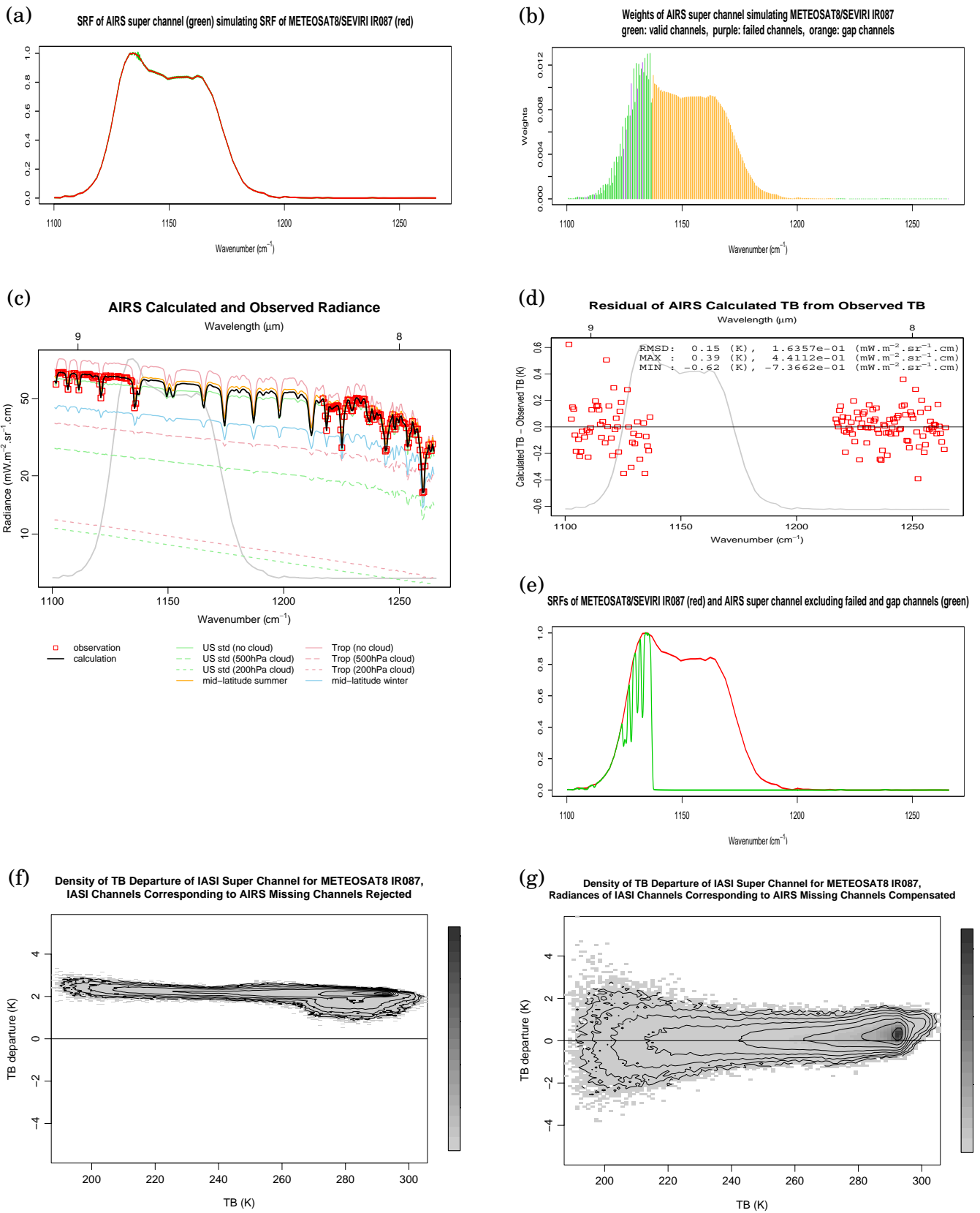


Figure 25: AIRS super channel simulating METEOSAT-8 $8.7 \mu\text{m}$ channel. The explanations of the charts are written in the Appendix body text.

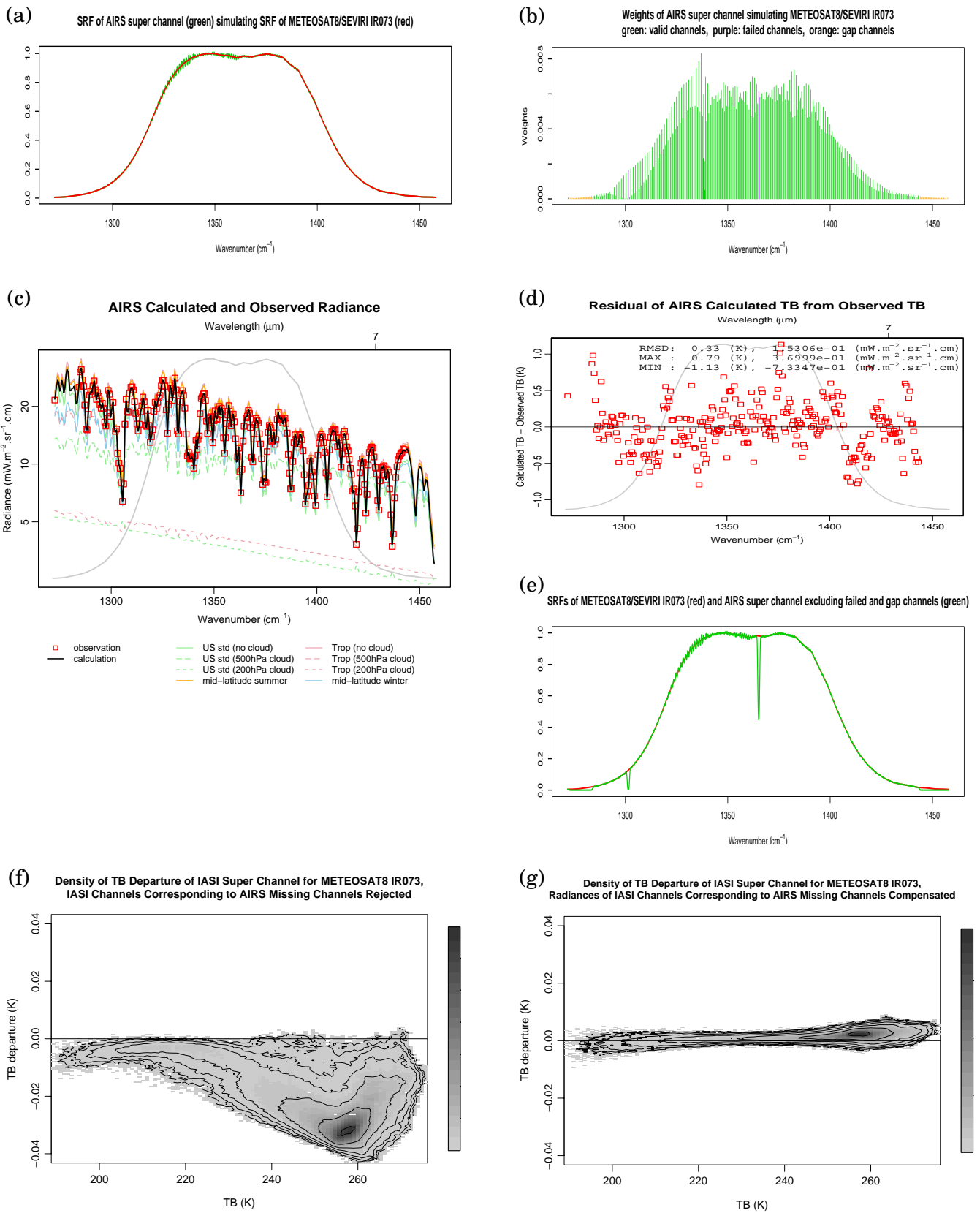


Figure 26: AIRS super channel simulating METEOSAT-8 $7.3 \mu\text{m}$ channel. The explanations of the charts are written in the Appendix body text.

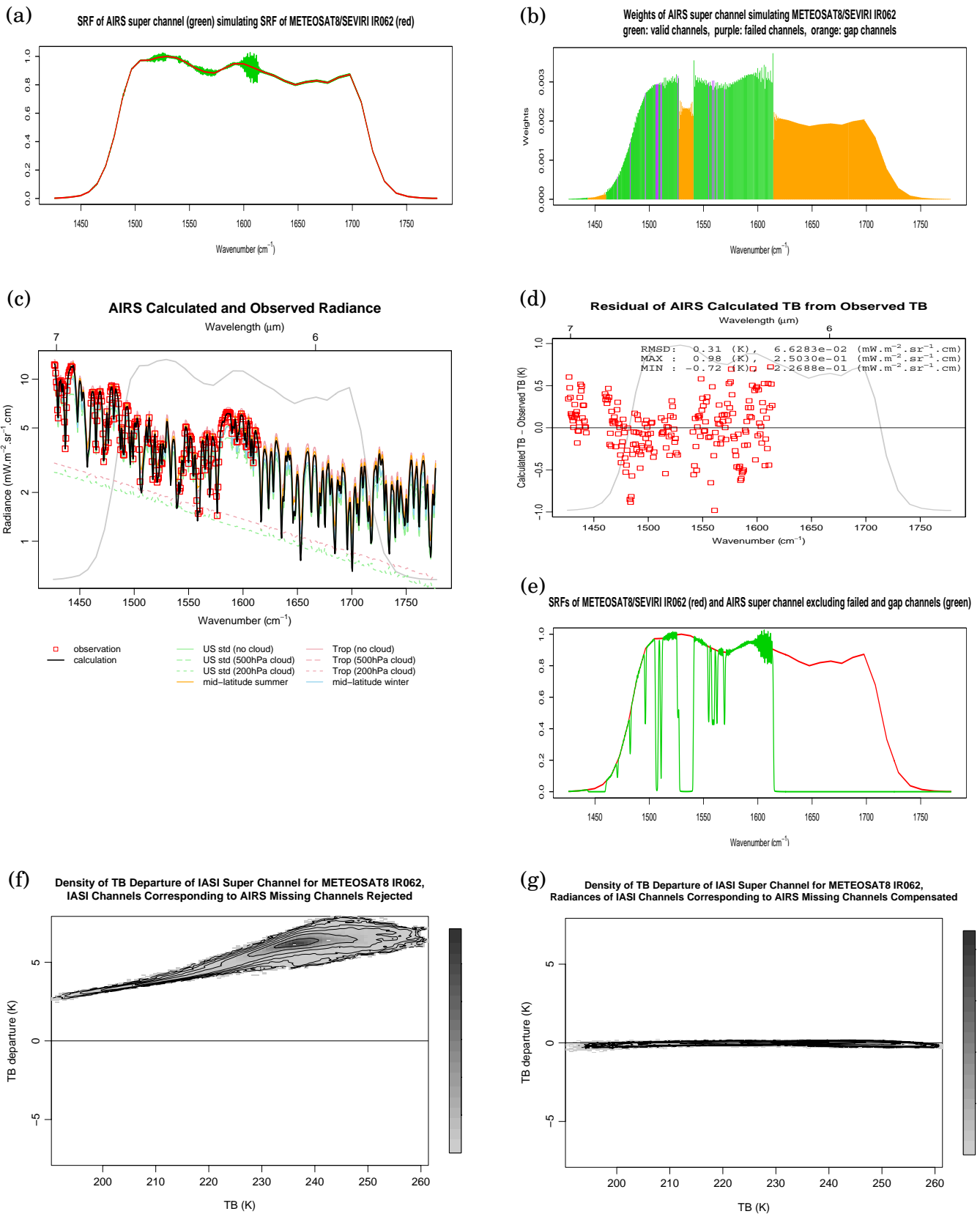


Figure 27: AIRS super channel simulating METEOSAT-8 6.2 μm channel. The explanations of the charts are written in the Appendix body text.

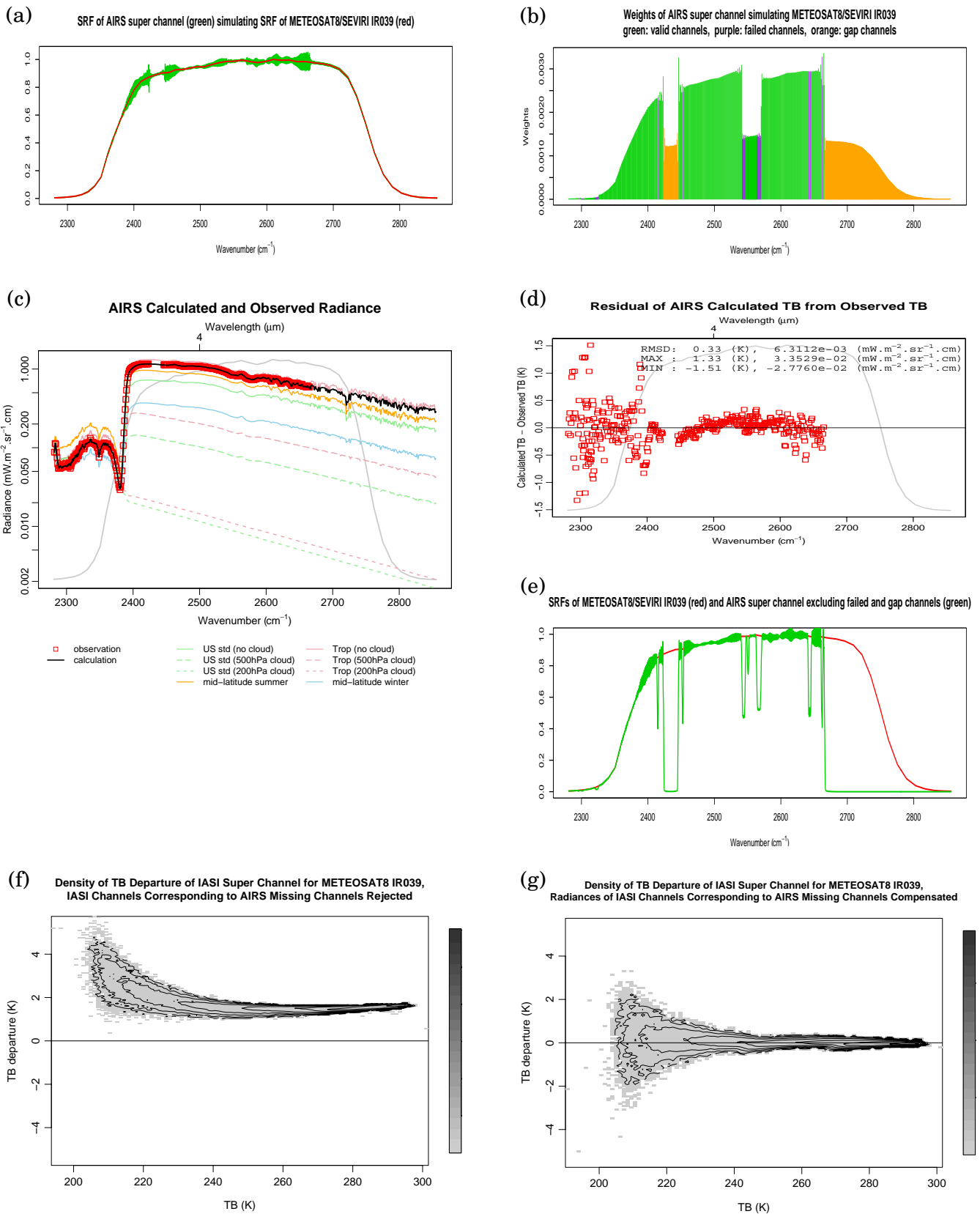


Figure 28: AIRS super channel simulating METEOSAT-8 3.9 μm channel. The explanations of the charts are written in the Appendix body text.

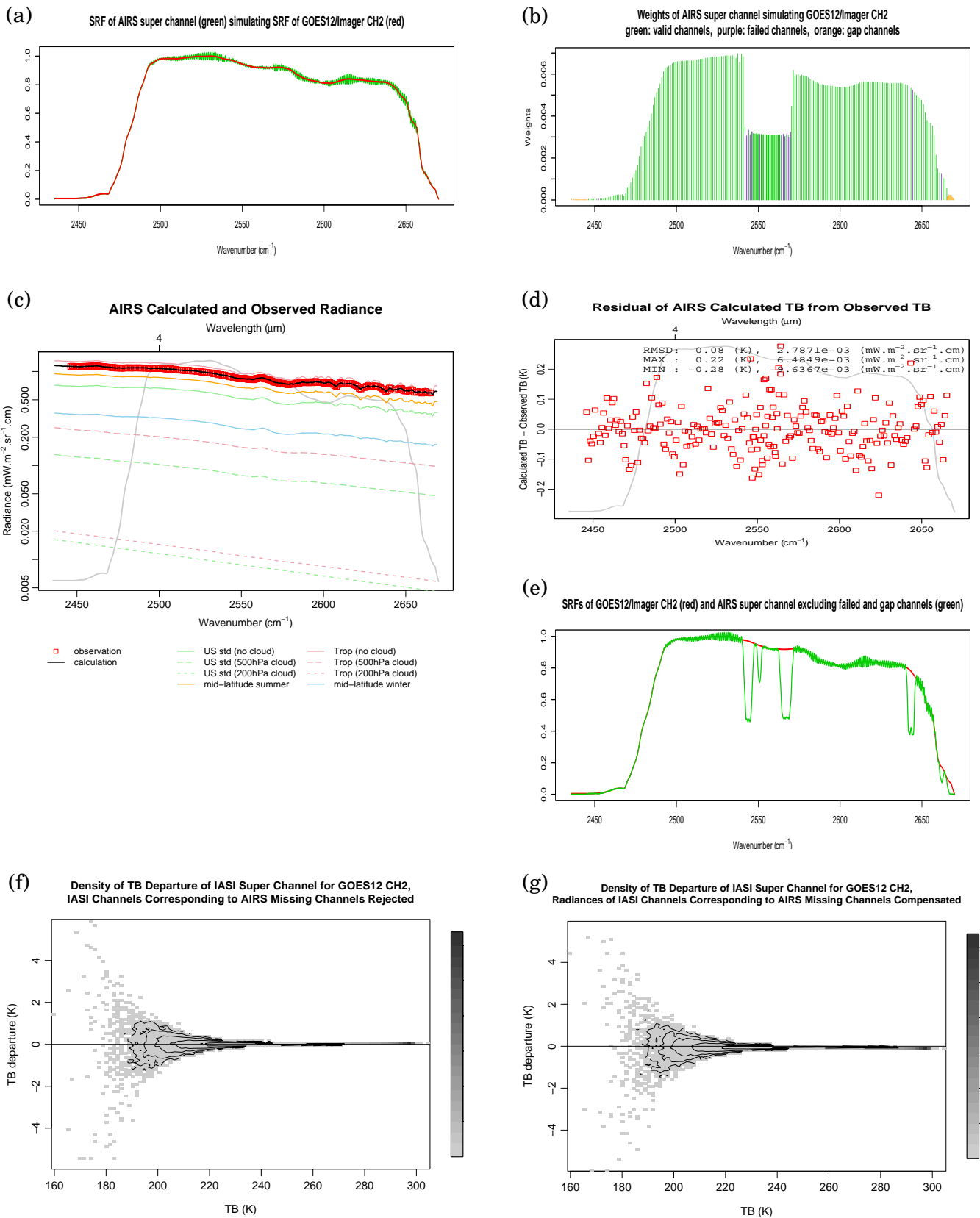


Figure 29: AIRS super channel simulating GOES-12 channel 2 (3.9 μm). The explanations of the charts are written in the Appendix body text.

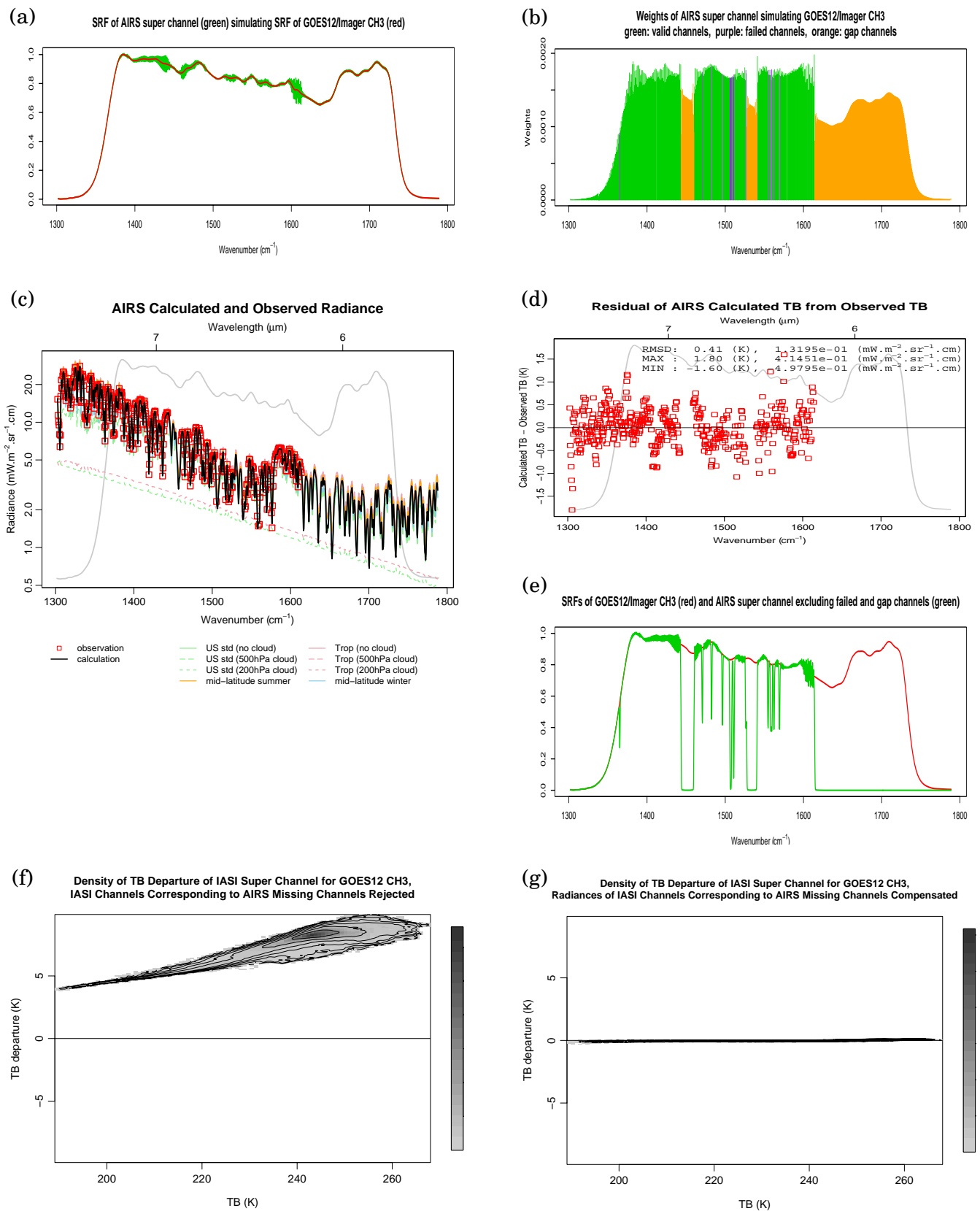


Figure 30: AIRS super channel simulating GOES-12 channel 3 ($6.5 \mu\text{m}$). The explanations of the charts are written in the Appendix body text.

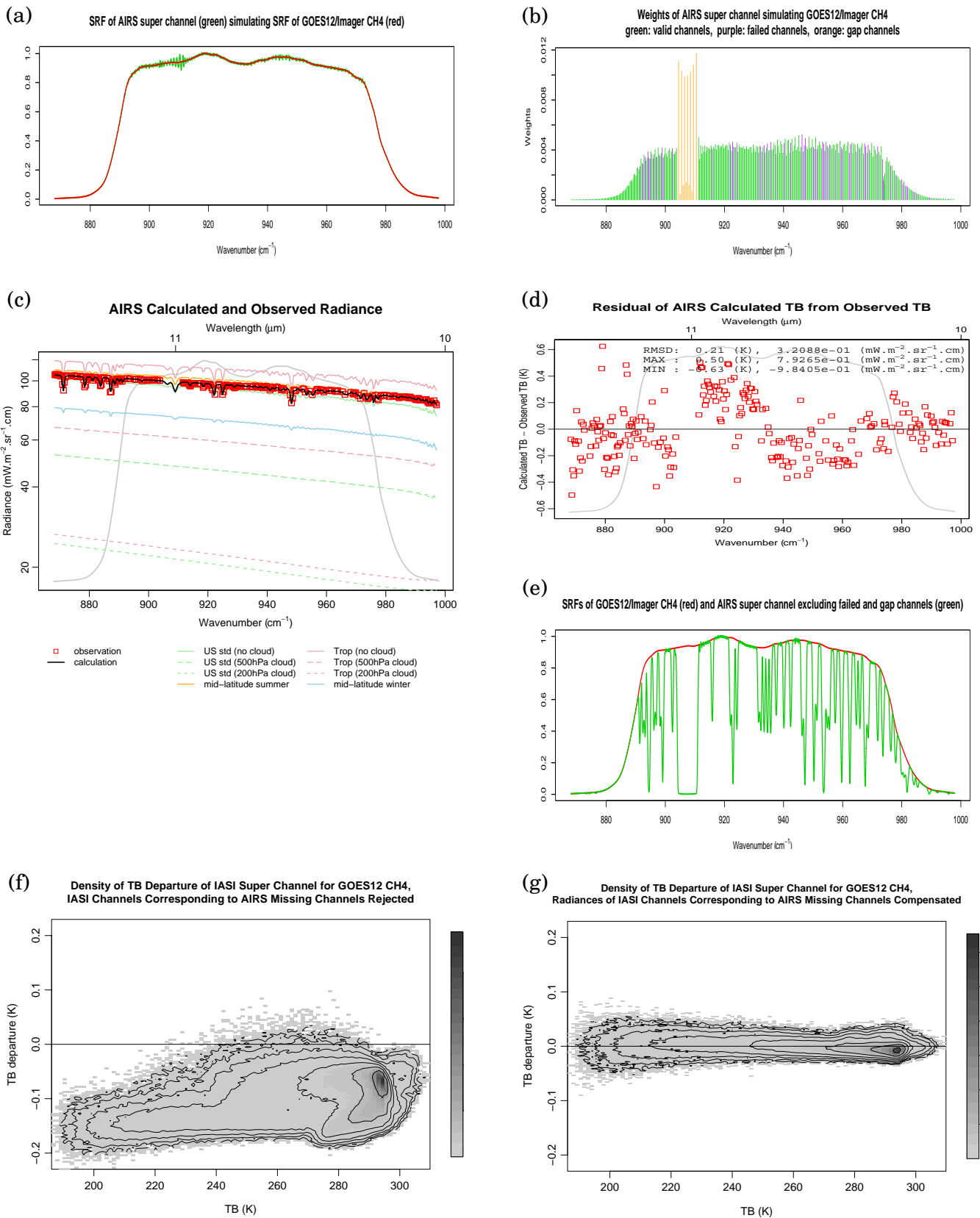


Figure 31: AIRS super channel simulating GOES-12 channel 4 (10.7 μm). The explanations of the charts are written in the Appendix body text.

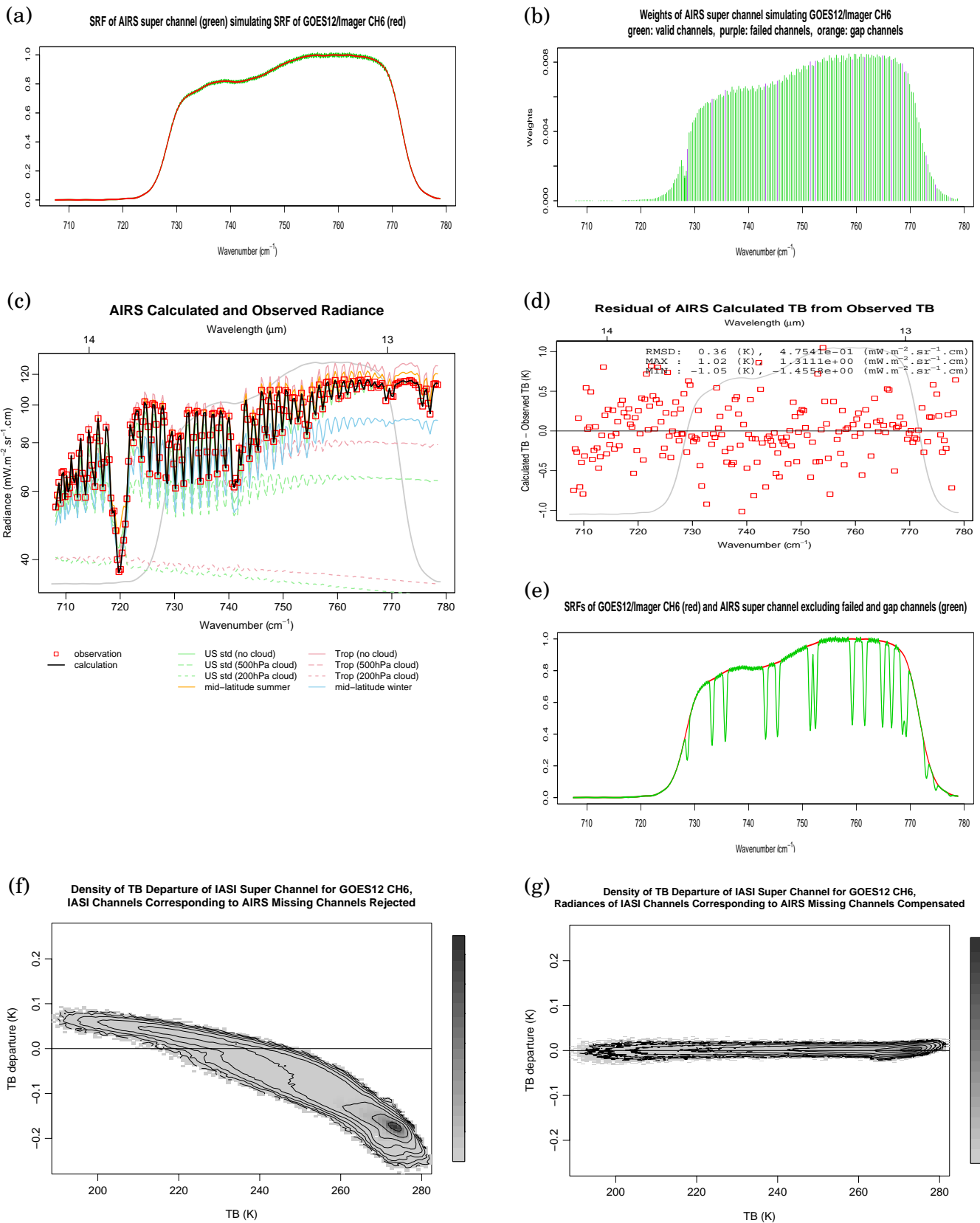


Figure 32: AIRS super channel simulating GOES-12 channel 6 ($13.3 \mu\text{m}$). The explanations of the charts are written in the Appendix body text.

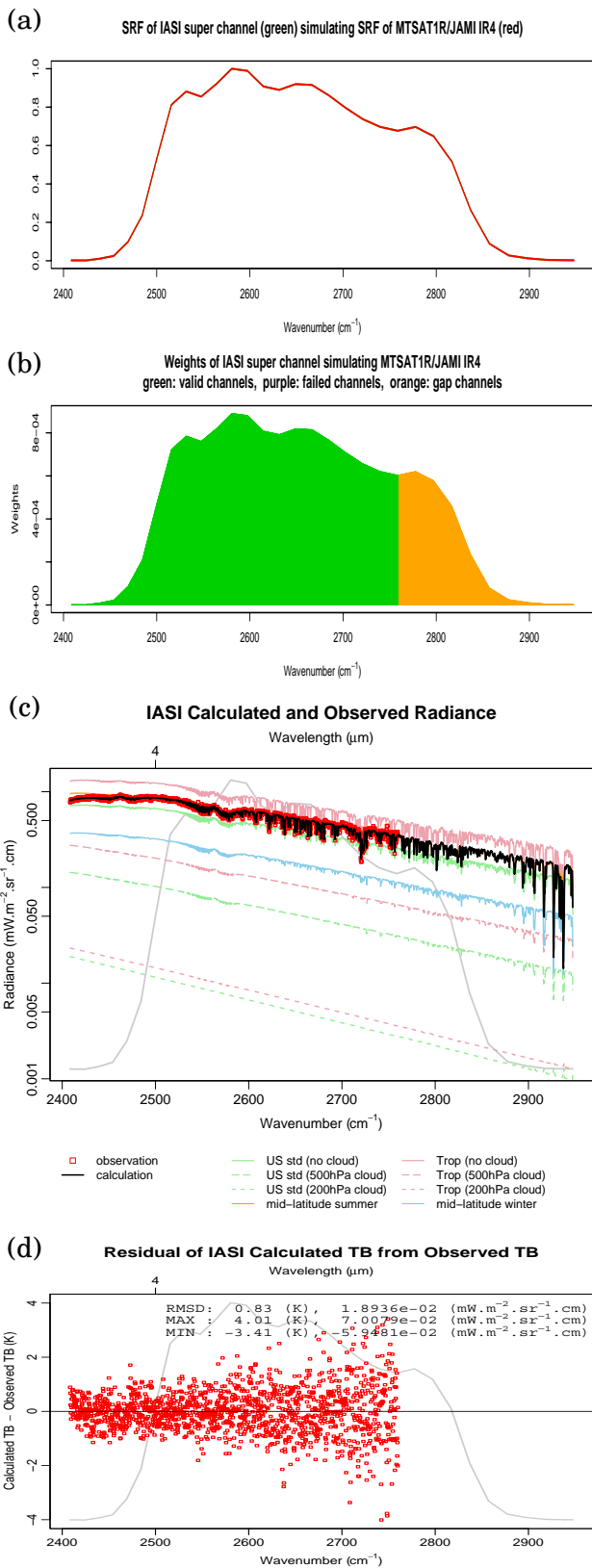


Figure 33: IASI super channel simulating MTSAT-1R channel IR4 ($3.8\ \mu\text{m}$). The explanations of the charts are written in the Appendix body text.

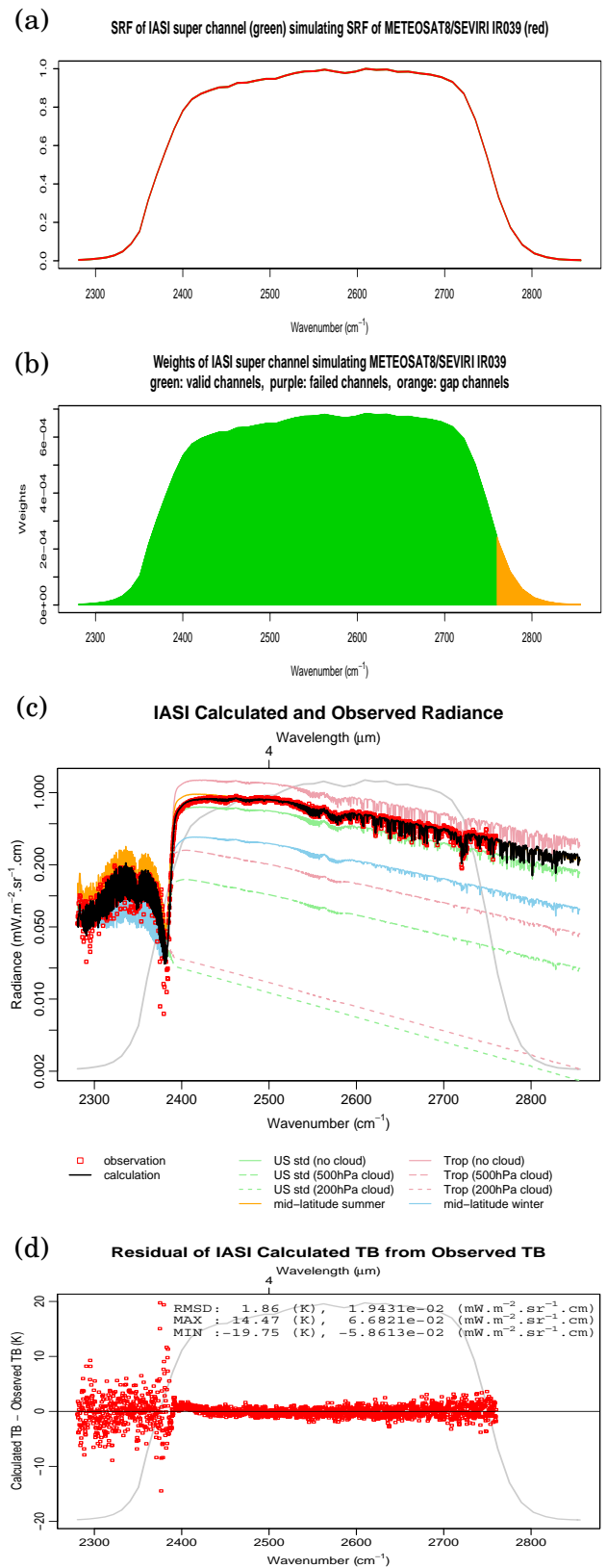


Figure 34: IASI super channel simulating METEOSAT-8 $3.9\ \mu\text{m}$ channel. The explanations of the charts are written in the Appendix body text.

高スペクトル分解能サウンドとのインターキャリブレーションに 必要な帯域補償に係る新手法

太原芳彦*、加藤浩司*

要旨

広い観測帯域を持つ静止気象衛星搭載のイメージャチャンネルと、高スペクトル分解能サウンド（ハイパーサウンド）とのインターキャリブレーションでは、ハイパーサウンドのチャンネル（ハイパーチャンネル）を合成したスーパーチャンネルが利用される。このスーパーチャンネルは、ハイパーチャンネルの不具合、観測帯域のすき間や不足がある場合、その品質が悪くなる。そのようなハイパーサウンドを利用するインターキャリブレーションでは、そのすき間や不足を補完する必要がある。そこで本研究では、まず「ギャップチャンネル」と呼ばれる疑似チャンネルを導入した。ギャップチャンネルを、不具合チャンネルも含めたハイパーチャンネルと共に利用することで、広帯域チャンネルのスペクトル応答とほぼ一致するスーパーチャンネルを作ることができた。次に、8つのモデル大気のスペクトル情報に基づくスペクトル補完手法を導入した。欠落チャンネル（ギャップチャンネルや不具合チャンネル）の放射は、そのモデル大気に関するシミュレート放射データを説明変数とする回帰計算で求めた。モデル大気には、熱帯と中緯度帯及び晴天と曇天の大気プロファイルを利用した。回帰係数は、ハイパーサウンドの観測放射データを目的変数に代入することで求めた。最後に、計算で求められた欠落チャンネルの放射データをハイパーサウンドの観測放射データと共に利用して、スーパーチャンネルの放射を求めた。本手法の利点は、事前のモデル大気に関する放射計算以外の放射計算が不必要であること、数値予報値を利用しないことにある。これにより、スーパーチャンネルの放射輝度計算において、数値予報値や放射計算に起因する系統誤差の混入を排除することができる。さらに、雲を含む事例についても利用できる。AIRSに見られる欠落チャンネルを、IASIチャンネルでシミュレートし、それらについて補完を試みた検証では、MTSAT-1RとMETEOSAT-8そしてGOES-12の全ての赤外チャンネルについて、欠落チャンネルで生じる系統誤差を減らす効果が確認された。2ヶ月間のデータを利用して行ったMTSAT-1R赤外チャンネルとAIRSのインターキャリブレーション結果は、本補完手法を利用することで、IASIとのインターキャリブレーション結果と合致することも確認された。

* 気象衛星センターデータ処理部システム管理課